Drosophila β-Tubulin 97EF is upregulated at low temperature and stabilizes microtubules

Myachina, Faina ; Bosshardt, Fritz ; Bischof, Johannes ; Kirschmann, Moritz ; Lehner, Christian F

DOI: https://doi.org/10.1242/dev.156109

Originally published at:
Myachina, Faina; Bosshardt, Fritz; Bischof, Johannes; Kirschmann, Moritz; Lehner, Christian F (2017). Drosophila β-Tubulin 97EF is upregulated at low temperature and stabilizes microtubules. Development, 144(24):4573-4587.
DOI: https://doi.org/10.1242/dev.156109

© 2017. Published by The Company of Biologists Ltd | Development (2017) 144, 4573-4587 doi:10.1242/dev.156109

RESEARCH ARTICLE

Drosophila β-Tubulin 97EF is upregulated at low temperature and stabilizes microtubules

Faina Myachina[1], Fritz Bosshardt[1], Johannes Bischof[1], Moritz Kirschmann[2] and Christian F. Lehner[1,*]

ABSTRACT

Cells in ectotherms function normally within an often wide temperature range. As temperature dependence is not uniform across all the distinct biological processes, acclimation presumably requires complex regulation. The molecular mechanisms that cope with the disruptive effects of temperature variation are still poorly understood. Interestingly, one of five different β-tubulin paralogs, *βTub97EF*, was among the genes upregulated at low temperature in cultured *Drosophila* cells. As microtubules are known to be cold sensitive, we analyzed whether *βTub97EF* protects microtubules at low temperatures. During development at the optimal temperature (25°C), *βTub97EF* was expressed in a tissue-specific pattern primarily in the gut. There, as well as in hemocytes, expression was increased at low temperature (14°C). Although *βTub97EF* mutants were viable and fertile at 25°C, their sensitivity within the well-tolerated range was slightly enhanced during embryogenesis specifically at low temperatures. Changing β-tubulin isoform ratios in hemocytes demonstrated that β-Tubulin 97EF has a pronounced microtubule stabilizing effect. Moreover, *βTub97EF* is required for normal microtubule stability in the gut. These results suggest that *βTub97EF* upregulation at low temperature contributes to acclimation by stabilizing microtubules.

KEY WORDS: Microtubules, Tubulin isoform, Boundary cells, Low temperature, Ectotherm

INTRODUCTION

Many ecological niches are exposed to ambient temperature fluctuations. Distinct strategies have evolved to cope with the disruptive effects of temperature changes on cellular homeostasis. Endotherms like humans rely primarily on internally generated heat for maintenance of a relatively high and constant core body temperature. However, the majority of organisms are ectotherms. Their internal temperature is primarily dictated by the environment. In addition, in endotherms, exposed peripheral cells need to function over a range of temperatures.

Arguably the most-extensive molecular analyses of low-temperature responses in eukaryotes have been carried out in yeast (Gasch et al., 2000; Taymaz-Nikerel et al., 2016), confirming the general notion that rapid temperature shifts to nonlethal low temperature disrupt cellular homeostasis, triggering an initial transient stress response followed by persistent acclimation. This low-temperature response is quite distinct from the general stress response induced by many other perturbations. In animals, low-temperature acclimation includes additional response levels (Denlinger and Lee, 2010; Hayward et al., 2007). Organ systems govern complex metabolic and behavioral responses.

At the cellular level, microtubules have long been recognized to be cold sensitive in mammals (Correia and Williams, 1983). Microtubules are dynamic cytoskeletal elements involved in innumerable processes (Nogales and Zhang, 2016). They are polymerized from heterodimers of α- and β-tubulin. Heterodimers can associate longitudinally into protofilaments. Lateral interactions between parallel protofilaments organize these into hollow cylindrical tubes. Both α- and β-tubulin bind GTP at a conserved site. GTP-tubulin heterodimers incorporate efficiently at growing microtubule ends. Polymerization is coupled to hydrolysis of GTP bound to β-tubulin. This regulates microtubule dynamics and gives rise to dynamic instability where growing phases alternate with shrinking phases (Mitchison and Kirschner, 1984; Zhang et al., 2015). Above a critical concentration, GTP-tubulin purified from mammalian sources polymerizes into microtubules at 37°C, largely driven by the entropically favorable displacement of structured water at the subunit interfaces (Correia and Williams, 1983). Reflecting the positive correlation between entropic drive and temperature, these microtubules depolymerize after a shift to 4°C in a GTP hydrolysis-independent manner (Fygenson et al., 1994).

Psychrophilic ectotherms assemble microtubules even below 0°C. Analysis of their genes has revealed amino acid changes that likely alter the temperature dependence of microtubule stability (Chiappori et al., 2012; Detrich et al., 2000; Modig et al., 2000; Tartaglia and Shain, 2008). Although such evolutionary adaptations support life at constant low temperature, organisms exposed to short-term thermal fluctuations presumably depend on temperature-controlled regulation of microtubule dynamics. In principle, regulated expression of tubulin paralogs with distinct properties is conceivable, as is control by post-translational modifications, microtubule-associated proteins (MAPs) and motors. Paralogs encoding distinct α- and β-tubulins have evolved in many lineages (Findeisen et al., 2014). Sequence differences are found predominantly in the C-terminal tails, where most post-translational modifications also occur. These modifications are thought to generate a 'tubulin-code' that controls binding and function of many MAPs and motors (Gadadhar et al., 2017; Janke, 2014; Sirajuddin et al., 2014; Yu et al., 2015).

In mammals, MAP6 adapts its conformation according to temperature to maintain microtubule networks in cells exposed to low temperature (Delphin et al., 2012). Moreover, the recent production of pure tubulin isoforms has definitely established inherent isoform-specific differences in microtubule dynamics *in vitro* (Pamula et al., 2016; Ti et al., 2016; Vemu et al., 2016).

Genetic analyses in *Drosophila melanogaster* have provided the first unequivocal evidence for paralog-specific functions *in vivo*

[1]Institute of Molecular Life Sciences (IMLS), University of Zurich, 8057 Zurich, Switzerland. [2]Center for Microscopy and Image Analysis, University of Zurich, 8057 Zurich, Switzerland.

*Author for correspondence (christian.lehner@imls.uzh.ch)

F.B., 0000-0002-1860-0050; C.F.L., 0000-0003-0185-6049

Received 21 June 2017; Accepted 20 October 2017

Development (2017) 144, 4573-4587 doi:10.1242/dev.156109

(Ludueña and Banerjee, 2008). The genome of *D. melanogaster* contains five α-tubulin genes, as well as five β-tubulin genes (*βTub56D*, *βTub60D*, *βTub85D*, *βTub97EF* and *CG32396*, designated here as *βTub65B*). The most divergent β-tubulin paralogs (*βTub85D* and *βTub65B*) are expressed exclusively in testis. Although *βTub65B* has not yet been studied, *βTub85D* has been characterized in considerable detail. It is required in the germline for male meiotic divisions and sperm axoneme formation (Fuller et al., 1988; Kemphues et al., 1982). These processes still fail when *βTub60D*, which is not normally expressed in the male germline, is expressed instead of *βTub85D* (Hoyle and Raff, 1990). The normal expression of *βTub60D* is also tissue specific, but considerably more complex than that of the testis-specific *βTub85D*. During embryogenesis, *βTub60D* expression starts in differentiating mesodermal cell types, but occurs also in chordotonal organs, imaginal discs and somatic cells of the adult gonads (Kimble et al., 1990; Rudolf et al., 2012). The zygotic expression of *βTub56D* has also pronounced tissue specificity, but at the start of embryogenesis the abundant maternal *βTub56D* contribution is the only source of β-tubulin (Buttgereit et al., 1996).

Here, we report that *βTub97EF*, an uncharacterized β-tubulin paralog, is upregulated at low temperature in specific cell types. Moreover, we demonstrate that it increases microtubule stability.

RESULTS

βTub97EF encodes a temperature-regulated β-tubulin

Genome-wide expression profiling with *Drosophila* S2R+ cells over a range of different growth temperatures revealed *βTub97EF* to be among the temperature-responsive genes. Compared with 25°C, the presumed optimal temperature, *βTub97EF* transcript levels were increased at lower temperatures (11 and 14°C) and decreased at a higher temperature (30°C) (Fig. 1A). In contrast to *βTub97EF*, other tubulin genes were at most marginally affected by growth temperature (Fig. 1A). Independent analyses with quantitative reverse transcription polymerase chain reaction (qRT-PCR) confirmed the microarray results (Fig. 1B,C). According to qRT-PCR, *βTub97EF* transcripts amount to about 8% of the total β-tubulin transcripts, whereas *βTub56D* and *βTub60D* contribute 46% each in S2R+ cells at 25°C (Fig. 1B). At 14°C, *βTub97EF* transcripts are more than twofold higher (Fig. 1C).

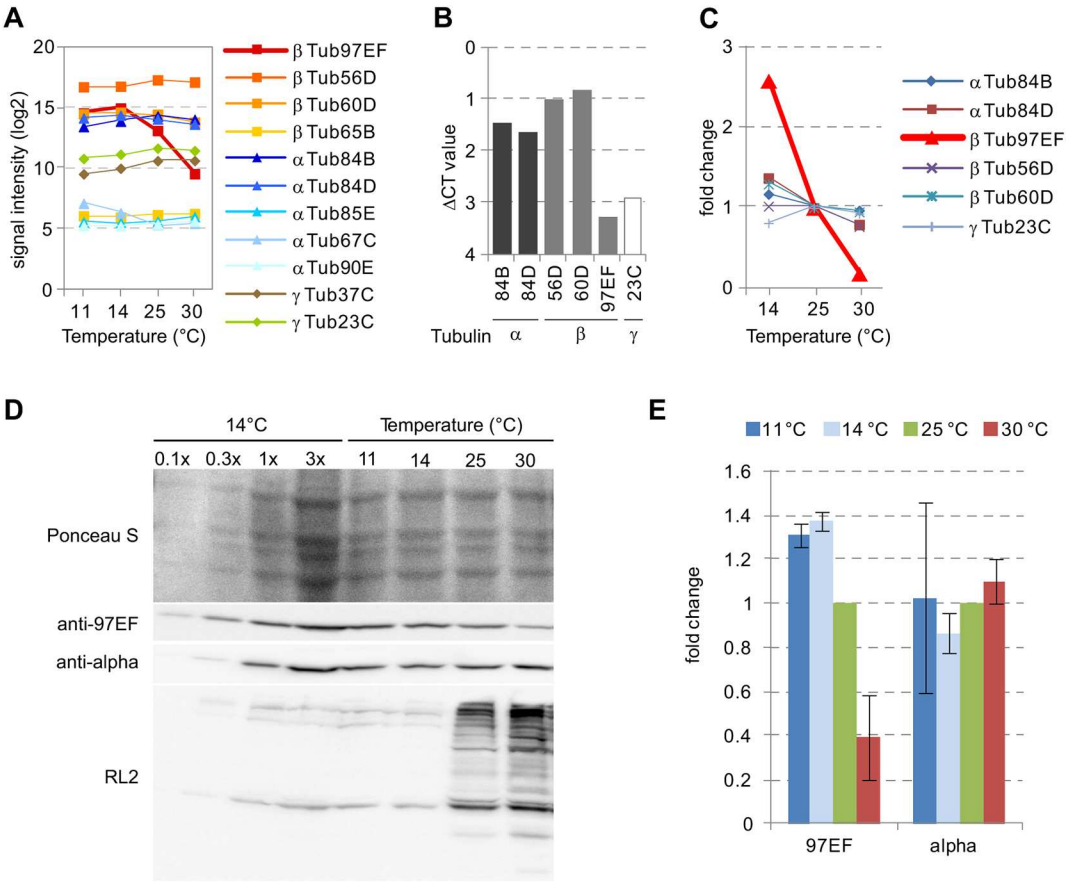

Fig. 1. *βTub97EF* expression is induced at low temperature. The effect of growth temperature on transcript and protein levels of *Drosophila* tubulin genes in S2R+ cells was analyzed using microarrays (A), qRT-PCR (B,C) or immunoblotting (D,E). (A) Temperature dependence of signal intensities on microarray probes. (B) Transcript levels of significantly expressed tubulin genes at 25°C. ΔCT values are indicated. A ΔCT value of zero indicates a transcript level equal to average expression of the genes used for normalization; higher ΔCT values indicate a relative decrease in expression. (C) Temperature dependence of transcript levels of significantly expressed tubulin genes. For each gene, the level at 25°C was set to 1. (D) Total extracts of S2R+ cells grown at 11, 14, 25 or 30°C were analyzed after western blotting by Ponceau S and probing with the indicated antibodies. RL2 detects O-GlcNAc modification on proteins, which is tightly correlated with growth temperature (Radermacher et al., 2014). Equal amounts of protein were loaded, except for the first four lanes covering a dilution series of the 14°C extract as internal reference for quantification. (E) Signals obtained with anti-β-Tubulin 97EF and anti-α-tubulin from immunoblots as shown in D were quantified. Ponceau S staining intensity was used for normalization. Signal intensities observed at 25°C were set to 1. Data are mean±s.d. (*n*=3).

Development (2017) 144, 4573-4587 doi:10.1242/dev.156109

To study temperature effects on protein abundance, we raised an antibody against β-Tubulin 97EF using a C-terminal peptide for immunization. The C-terminal tails are the most divergent regions of the highly conserved β-tubulins (Fig. S1). They have previously permitted production of paralog-specific antibodies (Kimble et al., 1989; Leiss et al., 1988). Immunoblotting experiments with extracts from bacteria expressing GST fusion proteins with extensions identical to the tails of the different β-tubulin paralogs were used for initial antibody characterization (Fig. S2A,B). Immunoblotting with these extracts also demonstrated that the mouse monoclonal antibody E7 (Chu and Klymkowsky, 1989) detects with almost equal sensitivity all of the β-tubulin paralogs, except β-Tubulin 65B, a most-divergent uncharacterized paralog with low testis-specific expression. The specificity of the newly generated antibodies for β-Tubulin 97EF was further confirmed by immunoblotting and immunolabeling experiments using *βTub97EF* mutants (see below). Quantitative immunoblotting indicated that the amount of β-Tubulin 97EF in S2R+ cells is only about 2% of the total β-tubulin protein at 25°C (Fig. S1C). However, although slightly less pronounced than in the case of *βTub97EF* transcripts, the protein was significantly more abundant in S2R+ cells at low temperature (11 and 14°C), and reduced at high temperature (30°C), compared with 25°C (Fig. 1D,E). As expected (Radermacher et al., 2014), control immunoblotting with RL2, an antibody recognizing O-GlcNAc-modified proteins, revealed the opposite temperature dependence. In conclusion, in cultured cells both mRNA and protein levels of *βTub97EF* respond to temperature. Higher levels are present at low temperatures.

βTub97EF expression occurs predominantly in the gut

Three of the five β-tubulin paralogs, *βTub56D*, *βTub60D* and *βTub85D*, have been studied in considerable detail (Rudolf et al., 2012 and references therein) but not *βTub97EF*. Therefore, the pattern of *βTub97EF* expression during development at 25°C was analyzed. By immunoblotting (Fig. 2A), β-Tubulin 97EF could not be detected at the onset of embryonic development, consistent with RNA-Seq data (Graveley et al., 2011). Zygotic expression started between 6-9 h after egg deposition (AED) and increased during the second half of embryogenesis. The specificity of the corresponding immunoblot signals (Fig. 2A) was confirmed with extracts of *βTub97EF* mutant embryos (see below).

For comparison, immunoblotting with anti-β-Tubulin 60D confirmed an expression program similar to β-Tubulin 97EF with a slightly earlier onset and peak of zygotic expression (Fig. 2A). Moreover, anti-pan-β-tubulin E7 revealed maximal levels of total β-tubulin at the start of embryogenesis (Fig. 2A) when the abundant maternally contributed β-Tubulin 56D is present (Rudolf et al., 2012). The monoclonal antibody DM1A (Blose et al., 1984) was used to detect α-tubulins (Fig. 2A). Based on its epitope characterization (Breitling and Little, 1986), DM1A presumably reacts with all or most of the *Drosophila* α-tubulins but the precise affinities for the different isoforms are not known.

Immunofluorescent labeling was performed to determine the spatial pattern of β-Tubulin 97EF expression during embryogenesis (Fig. 2B). β-Tubulin 97EF was not detected until stage 12, when weak specific signals were observed in the developing hindgut. Subsequently, signal intensities increased in the hindgut. Expression

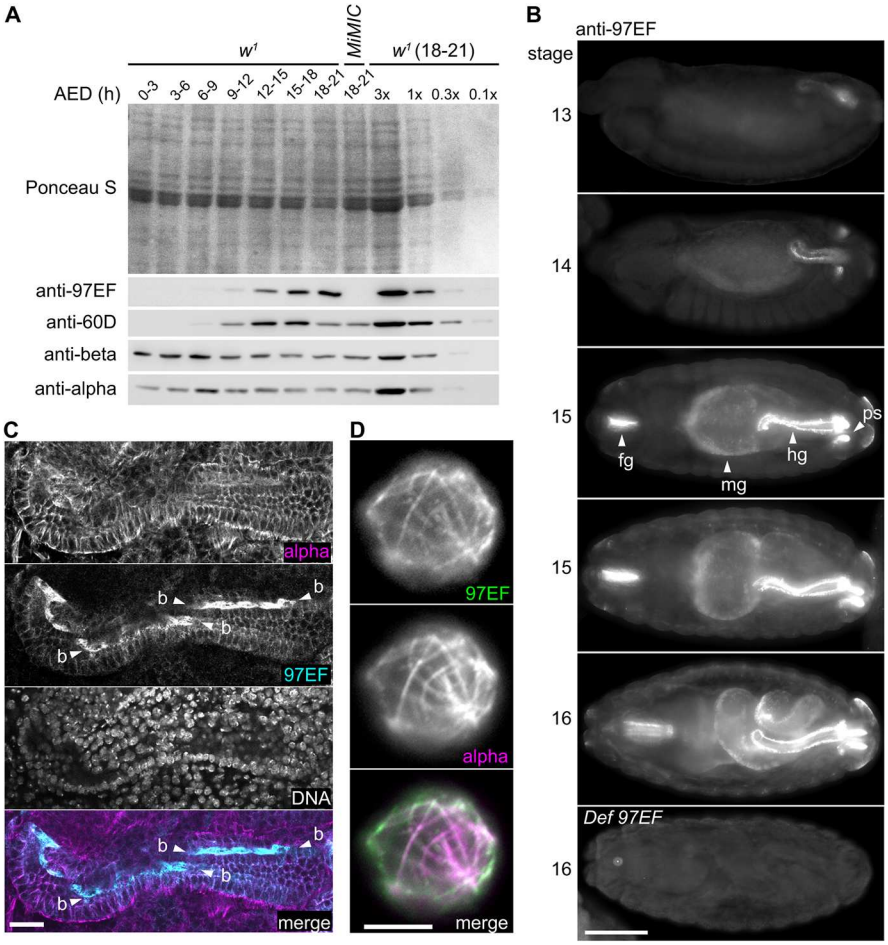

Fig. 2. *βTub97EF* expression during embryogenesis. (A) Total extracts from w^1 embryos at different ages AED. Equal numbers of embryos at each age interval were loaded apart from a dilution series. An extract from *βTub97EF* null mutants (*MiMIC*) was included. Ponceau S staining was used as a control for equal loading. Replicate immunoblots were probed with the indicated antibodies. (B) w^1 embryos were stained with anti-β-Tubulin 97EF and a DNA stain (not shown). In addition, an embryo homozygous for *Df(3R)BSC460*, which deletes *βTub97EF*, is shown in the bottom panel (*Def 97EF*). Numbers on the left indicate the displayed stages. Arrowheads indicate foregut (fg), midgut (mg), hindgut (hg) and posterior spiracles (ps). (C) Hindgut region (13-15 h AED) labeled as indicated. Boundary cells (b) are indicated by arrowheads. (D) Larval hemocyte after double labeling with anti-β-Tubulin 97EF and anti-α-tubulin. Scale bars: 50 µm in B; 10 µm in C; 5 µm in D.

Development (2017) 144, 4573-4587 doi:10.1242/dev.156109

was also detected in foregut and posterior spiracles, as well as more weakly in the midgut (Fig. 2B). The predominantly gut-specific expression pattern of β-Tubulin 97EF is clearly distinct from that of β-Tubulin 60D with its primarily muscle-specific expression pattern (Kimble et al., 1989; Leiss et al., 1988) (Fig. S3B). The maternally contributed, abundant β-Tubulin 56D is ubiquitously and uniformly distributed during embryogenesis, as indicated by E7 staining (Fig. S3A).

To characterize anti-β-Tubulin 97EF staining in further detail, the region with the embryonic hindgut was analyzed at high magnification (Fig. 2C). This revealed β-Tubulin 97EF in the epithelial cells of the hindgut, but not in the surrounding visceral muscles. Anti-β-Tubulin 60D resulted in the opposite pattern (Fig. S3C). Within the hindgut epithelium, β-Tubulin 97EF was most abundant in the so-called boundary cells (Fig. 2C), a row of single-cell width extending along both sides of the hindgut tube between the ventral and dorsal compartment (Iwaki and Lengyel, 2002).

At maximal resolution, near-perfect spatial overlap of the signals obtained by double labeling with anti-β-Tubulin 97EF and anti-α-tubulin was observed (Fig. 2D). For these high-resolution analyses, we used released larval hemocytes, which spread out on coverslips, providing superior optical conditions. Although β-Tubulin 97EF was colocalized with α-tubulin, the spatial intensity distributions of the signals obtained by double labeling with the two antibodies were not identical. Accordingly, β-Tubulin 97EF might be enriched in peripheral microtubules, but alternative explanations cannot be excluded (see Discussion).

Immunolabeling revealed that β-Tubulin 97EF is also present in the larval and adult gut (Fig. S4B,C). Signals in enterocytes were rather uniform, i.e. not as in the embryonic hindgut where boundary cells have higher levels. β-Tubulin 97EF was not only detected in the gut. Specific signals, although weaker, were observed in wing imaginal discs (also in spindles during mitosis), larval hemocytes and ovarial follicle cells (see below and data not shown).

We conclude that *βTub97EF* expression occurs in a pattern distinct from that of other β-tubulin paralogs. *In situ* hybridization and a *βTub97EF>EGFP* reporter allele suggested that tissue and cell-type specificity of *βTub97EF* expression is transcriptionally controlled (Fig. S3D,E).

βTub97EF upregulation by low temperature is tissue specific

To address the physiological role of *βTub97EF*, we characterized mutant alleles (Fig. 3A). Three *Minos* transposon insertions in the *βTub97EF* region were analyzed (Fig. 3A). PCR assays confirmed the annotated insertion positions. The insertion *Mi{MIC}βTub97EF^{MI06334}* within the first intron (*βTub97EF^{MiMIC}* in the following) introduces a splice acceptor site followed by translational stops in all three reading frames. By conversion of this insertion (Venken et al., 2011), a derivative with an extra EGFP-encoding exon within this first intron was obtained (*βTub97EF^{EGFP}*). The predicted protein product is expected to be non-functional because the EGFP insertion disrupts the tubulin core domain. Indeed, according to fluorescence microscopy, β-Tubulin 97EF^{EGFP} was not incorporated into microtubules.

By qRT-PCR (Fig. 3B) and immunoblotting (Fig. 3C), we analyzed how *βTub97EF* expression was affected by the transposon insertions. While two, *Mi{ET1}βTub97EF^{MB01877}* and *Mi{ET1}βTub97EF^{MB03812}*, reduced expression, *βTub97EF^{MiMIC}* appeared to abolish it completely (Fig. 3B,C). Residual β-Tubulin 97EF, potentially expressed from the *βTub97EF^{MiMIC}* allele, cannot be more than 3% of the normal level, because stronger expression would have been detectable (Fig. 3C). In the case of *βTub97EF^{EGFP}*, immunoblotting confirmed the expected expression of a larger β-Tubulin 97EF variant with an internal EGFP domain (Fig. 3C). As anti-β-Tubulin 97EF also revealed a weak band at the position of

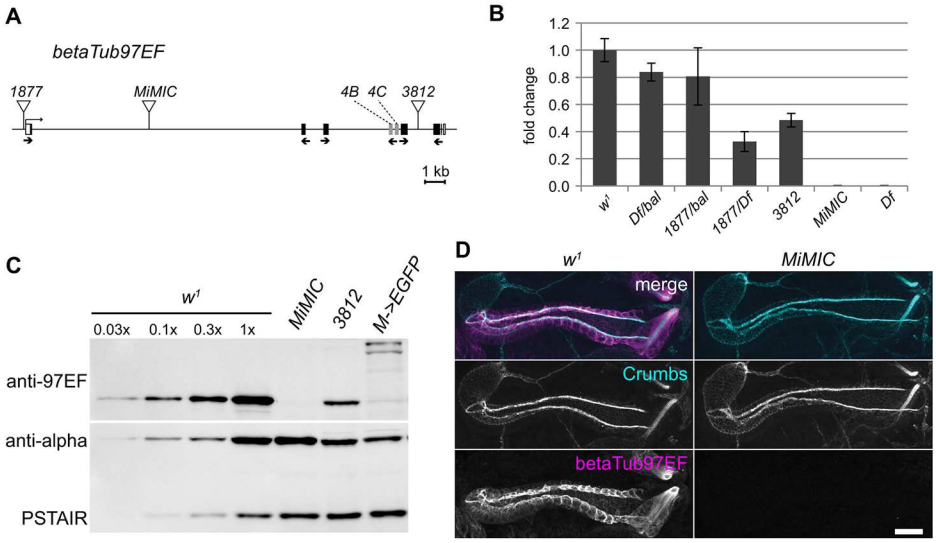

Fig. 3. Characterization of mutant *βTub97EF* alleles. (A) Scheme of the *βTub97EF* region. Transposon insertions (*1877*, *MiMIC* and *3812*) are indicated by triangles and exons by boxes with black filling in the coding region, except for the two mutually exclusive exons 4B and 4C, which are shown in gray. Small arrows below exons indicate the three primer pairs used for qRT-PCR. (B) *βTub97EF* transcript levels were determined by qRT-PCR using embryos of the indicated genotypes [*Df=Df(3R)BSC460*]. Results with the three primer pairs were highly concordant in a given genotype and were therefore averaged. Transcript levels are indicated by bars (mean±s.d., *n*=3 primer pairs). Those of w^1 control embryos were set to 1. (C) Total extracts from embryos (15-16 h AED) analyzed by immunoblotting with genotypes and antibodies indicated. Anti-α-tubulin and anti-PSTAIR were used as a mixture to probe the replicate immunoblot shown in the lower panel. (D) Hindgut region in embryos (14-15 h AED) after immunostaining with genotypes and antibodies as indicated. Crumbs is maximally expressed in the boundary cells of the hindgut. Scale bar: 20 µm.

Development (2017) 144, 4573-4587 doi:10.1242/dev.156109

normal β-Tubulin 97EF, the possibility of rare skipping of the extra EGFP exon present in the *βTub97EF*^{EGFP} allele cannot be excluded and might allow expression of normal β-Tubulin 97EF up to 10% of wild-type levels. Alternatively, the weak band might represent one of the obvious β-Tubulin 97EF^{EGFP} degradation products, rather than residual normal β-Tubulin 97EF.

Unexpectedly, given the conservation of the *βTub97EF* ortholog during an estimated 300 million years of insect evolution (Findeisen et al., 2014), *βTub97EF* function was found to be dispensable for viability and fertility under standard laboratory conditions. *βTub97EF*^{MiMIC} could be propagated as a homozygous stock. Compared with w^1, fertility was 25% lower in both sexes in flies with *βTub97EF*^{MiMIC} over a deficiency deleting *βTub97EF* [*Df(3R) BSC460*] (Fig. S5).

As *βTub97EF* expression is especially high in boundary cells of the embryonic hindgut, we analyzed whether these cells are present in *βTub97EF*^{MiMIC} mutants. Labeling of Crumbs, an apical membrane protein expressed at very high levels in boundary cells (Kumichel and Knust, 2014), demonstrated the presence of boundary cells in *βTub97EF*^{MiMIC} mutants (Fig. 3D). To compare hindgut morphology in *βTub97EF*^{MiMIC} mutants and control embryos with ultrastructural resolution, we applied focused ion-beam scanning electron microscopy (FIBSEM). Although this failed to expose abnormalities in *βTub97EF*^{MiMIC} mutants, our three-dimensional reconstructions revealed that boundary cells differentiate striking undulae propagating longitudinally from cell to cell along the hindgut epithelial tube (Fig. S6), rather than prominent microvilli as suggested previously based on two-dimensional EM analyses (Iwaki and Lengyel, 2002; Kumichel and Knust, 2014; Soplop et al., 2012).

The hindgut is one of the organs that develops left/right asymmetry during development (Coutelis et al., 2014). *βTub97EF*^{MiMIC} mutants were found to have normal left/right asymmetry in larval and adult hindgut (Fig. S5). We also addressed whether absence of β-Tubulin 97EF from the gut might increase sensitivity to hyperosmotic diet. Therefore, survival to the adult stage after larval development in high-salt food was analyzed. However, *βTub97EF*^{MiMIC} mutants were not more salt-sensitive than w^1 control (Fig. S5).

Our phenotypic analyses suggested that *βTub97EF* does not provide crucial functions at temperatures close to the optimum of 25°C. However, as *βTub97EF* expression is increased in S2R+ cells at low temperature (Fig. 1), this gene might be of a greater importance during development and life at sub-optimal temperatures. First we analyzed whether regulation of *βTub97EF* expression by temperature occurs also in embryos. After egg collection at 25°C, aliquots were shifted at 3-6 h AED (i.e. before the onset of *βTub97EF* expression) to either 14, 25 or 30°C. Once embryos had reached stage 16 (peak of *βTub97EF* expression), total RNA was analyzed by qRT-PCR. Among tubulin paralogs, *βTub97EF* is unique with regard to the presence of two mutually exclusive exons (4B and 4C) within the region coding for the conserved tubulin protein core (Fig. 3A) (Findeisen et al., 2014). These two mutually exclusive exons appear to be characteristic for dipterans (Findeisen et al., 2014). In *D. melanogaster* they share 77% identity at the amino acid sequence level (Fig. S1). Based on splice junction counts (Graveley et al., 2011), the 4B variant is about 15-fold more abundant than the 4C variant throughout development. Our qRT-PCR analyses were carried out with two distinct primer pairs designed to detect specifically one or the other isoform. While the minor 4C transcripts were found to be downregulated, the major 4B transcripts were upregulated at lower temperature (11°C) (Fig. 4A).

Aliquots of the same embryos were also analyzed by immunoblotting (Fig. 4B). This confirmed that β-Tubulin 97EF protein was upregulated after development at low temperature. On average, β-Tubulin 97EF levels were fourfold higher at 14°C compared with 30°C (Fig. 4B). Although with variation in extent, higher β-Tubulin 97EF levels at the lower temperature were consistently observed in each of three experiments. In contrast, signals obtained by immunoblotting with anti-β-Tubulin 60D and anti-α-tubulin were not affected by temperature (Fig. 4B), indicating that induction by low temperature is specific for the *βTub97EF* paralog.

To address whether the upregulation of β-Tubulin 97EF at low temperature occurs globally or in a tissue-specific manner, we performed quantitative immunofluorescent labeling. Quantification of the specific, background-corrected anti-β-Tubulin 97EF signals indicated that β-Tubulin 97EF levels were 1.7-fold higher in the embryonic hindgut at 14°C compared with 25°C, and twofold higher when compared with 30°C (Fig. 4C,D). In contrast, anti-α-tubulin signals were not affected by temperature (Fig. 4C,D). Analogous quantification of signals within epidermis and somatic muscles did not reveal any temperature effects on either β-Tubulin 97EF or α-tubulin signals (Fig. S7).

Although low temperature induces higher β-Tubulin 97EF levels in the hindgut, this organ appeared to be morphologically normal in *βTub97EF*^{MiMIC} mutants even after embryonic development at 14°C or 12°C (data not shown). Despite normal morphology, certain cells or tissues might not be fully functional in *βTub97EF*^{MiMIC} mutants. Therefore, we analyzed temperature sensitivity of development to the larval and adult stages. Embryos were collected at 25°C and aliquots were shifted after gastrulation, but before the onset of *βTub97EF* expression, to temperatures within the range of 10 to 34°C (Fig. 4E). The rate of larval hatching from eggs (Fig. 4F) as well as the rate of development to the adult stage was determined (Fig. 4G). At the lowest temperature analyzed (10°C), no larvae hatched from either control or *βTub97EF* mutant eggs. Similarly, only very few larvae hatched at 11°C and 12°C (Fig. 4F). Interestingly, at 14°C, 25% fewer *βTub97EF*^{MiMIC} mutants completed embryogenesis successfully compared with control (Fig. 4F). This temperature of 14°C is the lower limit for completion of the entire life cycle for standard *D. melanogaster* laboratory strains. Therefore, *βTub97EF* function appears to be important at the lower end of the temperature range compatible with the complete life cycle. In contrast, at 30°C, the upper end of this compatible range, there were no significant survival differences between *βTub97EF*^{MiMIC} mutants and control, as also at the optimum temperature of 25°C (Fig. 4F). At temperatures above the range compatible with the complete life cycle (32, 33 and 34°C), embryogenesis of *βTub97EF* mutants was less successful than in controls (Fig. 4F).

When analyzing development up to the adult stage, *βTub97EF* mutants were found to be significantly weaker than control, at temperatures below as well as above the optimum (Fig. 4G). By immunoblotting with total larval extracts, we were actually unable to detect β-Tubulin 97EF upregulation at low temperature at this developmental stage (data not shown). In conclusion, within the temperature range where the full *D. melanogaster* life cycle can be completed, *βTub97EF* function is more important for successful embryogenesis at the lower than at the upper limit, supporting the notion that *βTub97EF* upregulation at low temperature contributes to acclimation. However, at more extreme temperatures and during larval and pupal development, *βTub97EF* does not appear to be more crucial for cold compared with heat survival.

Development (2017) 144, 4573-4587 doi:10.1242/dev.156109

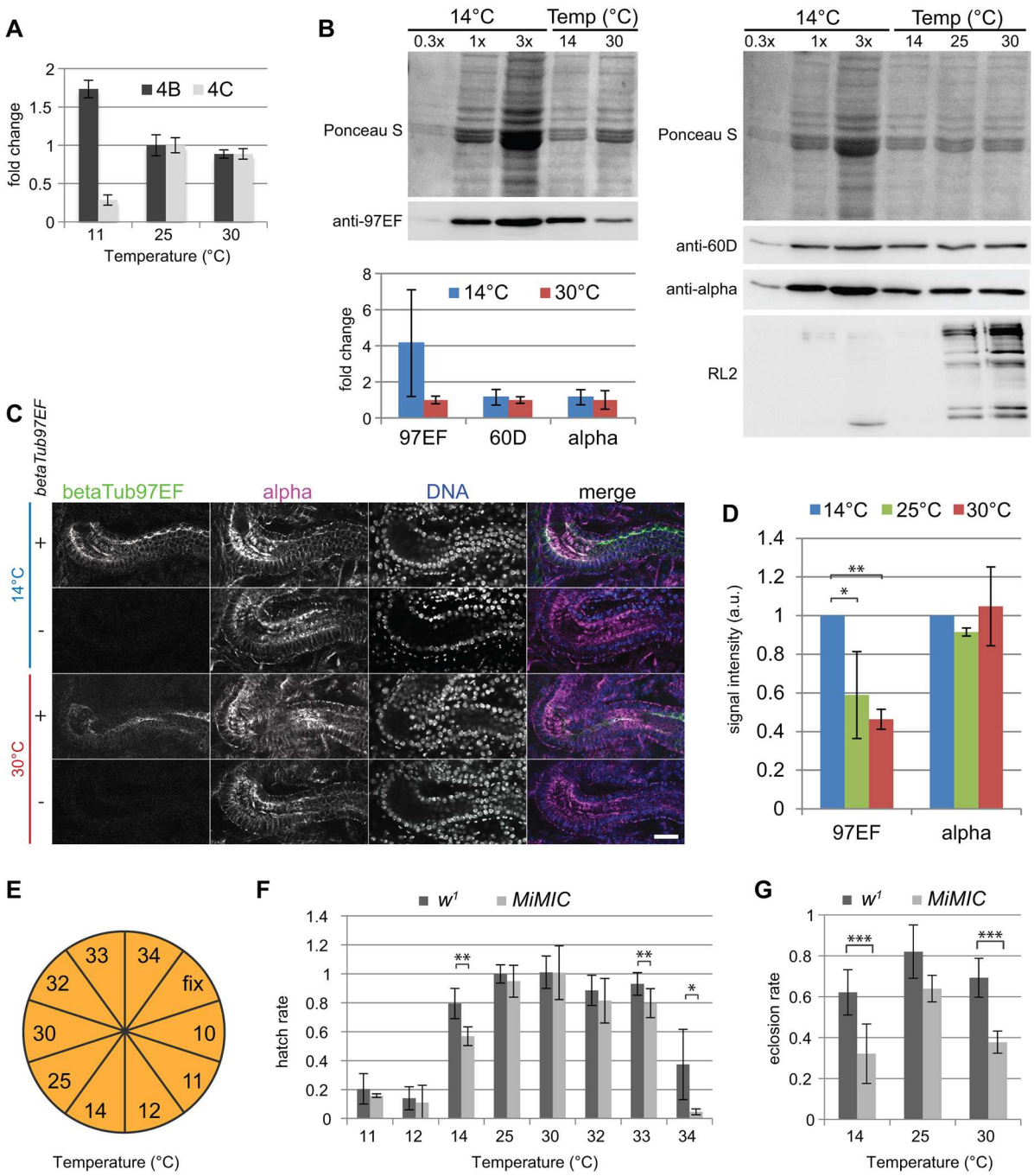

Fig. 4. *βTub97EF* upregulation at low temperature in embryos is tissue specific. (A) qRT-PCR revealed that the major *βTub97EF* transcript isoform with exon 4B is upregulated at low temperature, whereas the minor alternative transcript with exon 4C is downregulated. Expression levels at 25°C were set to 1. Data are mean±s.d. (*n*=3 technical replicates). (B) Immunoblotting revealed that β-Tubulin 97EF protein is upregulated in embryos at low temperature, in contrast to β-Tubulin 60D and α-tubulin. Data are mean immunoblot signal intensities at 14° and 30°C (±s.d.; *n*=3 biological replicates). Ponceau S staining intensity was used for normalization. Intensities observed at 30°C were set to 1. (C,D) Upregulation of β-Tubulin 97EF at low temperature is tissue specific. (C) Confocal sections through hindgut illustrate labeling with the indicated antibodies and DNA staining in embryos of the indicated genotypes after development at 14°C and 30°C, respectively. Scale bar: 20 µm. (D) Quantification of signal intensities obtained with anti-β-Tubulin 97EF and anti-α-tubulin in the hindgut epithelium. Expression levels observed at 14°C were set to 1. Data are mean±s.d. (*n*=6 embryos). (E-G) Temperature sensitivity of development of the *βTub97EF* mutant. (E) Experimental strategy for the analyses at different temperatures. Egg collections were divided into aliquots and incubated at the indicated temperatures. One part (fix) was used for the determination of the number of unfertilized and overaged embryos. (F) Rate of larval hatching at different temperatures. (G) Rate of development to the adult stage at different temperatures. Data are mean±s.d. (*n*=3). **P*<0.05, ***P*<0.01, ****P*<0.001 (*t*-test).

The core and C-terminal tail domains contribute to functional specialization of β-Tubulin 97EF

Functional redundancy of co-expressed β-tubulin paralogs might explain the mild phenotypic consequences of *βTub97EF* null mutations. In *βTub97EF* mutant embryos, the maternally provided abundant β-Tubulin 56D (Buttgereit et al., 1991) is present at least initially. To address potential functional redundancy, we first characterized *βTub56D* mutant alleles. We studied two transposon

Development (2017) 144, 4573-4587 doi:10.1242/dev.156109

insertions, $\beta Tub56D^{NP0949}$ and $\beta Tub56D^{EY12330}$, that appeared likely to be detrimental for *βTub56D* function (Fig. 5A). Both insertions were found to be homozygous lethal, as well as over a deficiency [*Df(2R)BSC782*] that eliminates 5′ upstream sequences, promoter region and the first *βTub56D* exon (Fig. 5A). Moreover, the two transposon insertions failed to complement each other. Finally, the developmental lethality associated with $\beta Tub56D^{NP0949}/Df(2R)BSC782$ was completely suppressed by

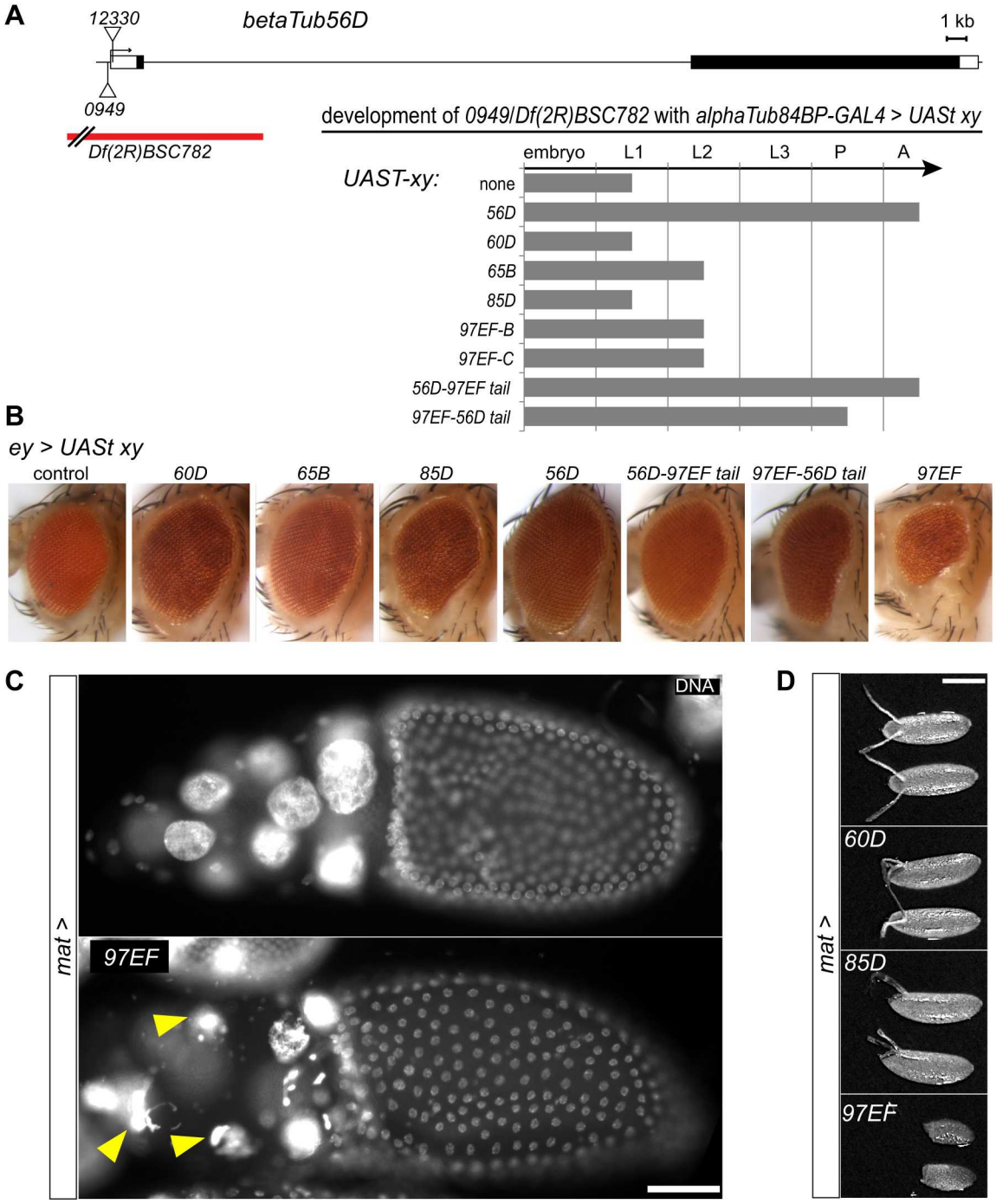

Fig. 5. Functional specialization of β-Tubulin 97EF. (A-C) Functional specialization was addressed by complementation experiments involving expression of β-tubulin paralogs in *βTub56D* mutants (A) as well as after ectopic expression (B,C). (A) The P-element insertions *NP0949* and *EY12330* within the *βTub56D* region are indicated (triangles), as well as the intragenic breakpoint of the deficiency *Df(2R)BSC782*. Exons are represented by boxes with black filling indicating coding region. Gray bars indicate the extent of development of $\beta Tub56D^{NP0949}/Df(2R)BSC782$ mutants with *αTub84BP-GAL4*-driven expression of the indicated *UASt-β-tubulin* transgenes. Around 100 larvae were scored for each genotype. Larval instar stage 1-3 (L1-L3), pupal stage (*P*) and adult stage (A). (B) Eye phenotype in adults after *ey-GAL4*-driven expression of the indicated *UASt-β-tubulin* transgenes. (C,D) *matα4-GAL4VP16* was used for expression of the indicated *UASp-β-tubulin* transgenes during oogenesis. (C) DNA staining in stage 10B egg chambers. Arrowheads indicate some of the abnormal nurse cell nuclei. (D) Morphology of deposited eggs. Scale bars: 50 µm.

Development (2017) 144, 4573-4587 doi:10.1242/dev.156109

UASt-βTub56D expression driven by *αTub84BP-GAL4* (Fig. 5A). Therefore, $βTub56D^{NP0949}$ and $βTub56D^{EY12330}$ are loss-of-function alleles of *βTub56D*.

The lethality associated with $βTub56D^{NP0949}/Df(2R)BSC782$ occurred after embryogenesis during the first larval instar (Fig. 5A, Fig. S8), suggesting that the maternal *βTub56D* contribution is sufficient for successful completion of embryogenesis. Indeed, the abundant maternal *βTub56D* contribution was found to be stable throughout embryogenesis, as revealed by immunolabeling experiments using *Df(2R)BSC782* (Fig. S8). This maternal *βTub56D* contribution might explain why hindgut development appeared to be normal even when zygotic function of both *βTub97EF* and *βTub56D* were missing during embryogenesis (data not shown).

Paralog retention after gene duplication during evolution usually depends on functional specialization at the level of expression and/or protein function. To address protein specialization, we compared the *βTub56D* mutant rescue potential of the different β-tubulin paralogs (Fig. 5A). For paralog expression in *βTub56D* mutants [$βTub56D^{NP0949}/Df(2R)BSC782$], we always used the same *GAL4* driver (*αTub84BP-GAL4*) in combination with *UASt* transgenes that differed within only the coding region. The coding region was that of the β-tubulin paralogs 56D, 60D, 65B, 85D and 97EF, with either exon 4B or 4C. As described above, *UASt-βTub56D* expression resulted in complete rescue of $βTub56D^{NP0949}/Df(2R)BSC782$ first instar larval lethality (Fig. 5A). In contrast, *UASt-βTub97EF(4B)* and *UASt-βTub97EF(4C)* provided only limited rescue. Lethality still occurred, but during the second larval instar rather than during the first (Fig. 5A). Although such a partial rescue was also obtained with *UASt-βTub65B*, the others (*UASt-βTub60D* and *UASt-βTub85D*) did not appear to cause rescue (Fig. 5A).

Additional experiments with the *UASt* transgenes revealed that ectopic expression of some β-tubulin paralogs is highly toxic in an otherwise normal background. When the *UASt* transgenes were expressed with *ey-GAL4* during eye development, for example (Fig. 5B), the β-Tubulin 97EF isoforms were more toxic than all the other β-tubulin paralogs. Although the variant with the 4C exon was lethal, the 4B version resulted in small deformed and rough eyes, indicating that the two β-Tubulin 97EF isoforms are functionally distinct.

When *matα4-GAL-VP16* was used to drive *UASp-βTub97EF(4B)* during oogenesis, female sterility was observed and the dumping of nurse cell cytoplasm into the oocyte that normally occurs during stage 10B was inhibited (Fig. 5C,D). Such a dumpless egg chamber phenotype was not obtained with *UASp-βTub85D* or *UASp-βTub60D* (Fig. 5D). Immunolabeling confirmed that ectopic expression of both the toxic β-Tubulin 97EF and the non-toxic β-Tubulin 60D occurred as expected in the germline, starting during stage 2 (Fig. S9). During wild-type oogenesis, both β-Tubulin 97EF and β-Tubulin 60D are normally expressed in somatic follicle cells but not in the germline (Fig. S9).

The C-terminal tails (CTTs) of tubulin paralogs are the most divergent region, and different types of post-translational modifications occur predominantly in this region, potentially generating a tubulin code that might direct interactions with specific sets of MAPs and motor proteins. To evaluate whether the functional difference between β-Tubulin 97EF(4B) and β-Tubulin 56D reflects sequence changes within core or CTT, we performed *βTub56D* mutant rescue experiments with *UASt* transgene encoding tail-swapped variants. This assay indicated that the functional difference between β-Tubulin 97EF(4B) and β-Tubulin 56D reflects alterations within both core and CTT (Fig. 5A). We conclude that *βTub97EF* is not just expressed in a specific pattern but that it also codes for a β-tubulin with unique functions as a result of sequence changes within both the tubulin core and CTT.

β-Tubulin 97EF generates stable microtubules

For further analysis of the functional differences between β-Tubulin 97EF and β-Tubulin 56D, we studied larval hemocytes. As S2R+ cells have an expression profile most similar to hemocytes (Cherbas et al., 2011), it appeared likely that larval hemocytes express *βTub97EF* in a temperature-regulated manner. Indeed, immunolabeling confirmed that larval hemocytes do not only express *βTub56D* but also *βTub97EF* (Fig. 2D and Fig. 6A). Moreover, the β-Tubulin 97EF level was significantly increased at 14°C compared with 29°C (Fig. 6B). By exploiting larval hemocytes from *βTub56D* mutants in combination with expression of *UASt* tubulin transgenes, we were able to alter the relative abundance of β-Tubulin 97EF and β-Tubulin 56D even at the optimal temperature of 25°C (Fig. 6A). Moreover, co-expression of *UASp-EB1-GFP* allowed quantitative analyses of some aspects of microtubule dynamics *in vivo*. EB1-GFP accumulates on the plus ends of growing microtubules (Mimori-Kiyosue et al., 2000). Therefore, we used hemocytes from *βTub56D* mutant second instar larvae expressing *UASt-βTub97EF(4B)* or *UASt-βTub56D*, and in some of the experiments also *UASp-EB1-GFP* driven by *αTub84BP-GAL4*. In the following, these hemocytes will be designated as *R-97EF* and *R-56D* (rescued by the 97EF and 56D paralog, respectively). In addition, we also analyzed hemocytes from siblings (*S-97EF* and *S-56D*, respectively), which expressed the *UAS* transgenes in balanced *Df(2R)BSC782* larvae with a functional endogenous *βTub56D* copy on the balancer.

After immunolabeling, we quantified the signals obtained with anti-β-Tubulin 97EF, anti-α-tubulin (DM1A) and anti-β-tubulin (E7) in the hemocytes (Fig. 6A). We point out that these signals primarily reflect the polymerized tubulin pool rather than the total cellular pool. Fixation seems to result in a loss of soluble tubulin, as suggested by the comparison of anti-tubulin immunolabeling signal intensities after brief pretreatment with either microtubule inhibitors (nocodazole, vinblastine) or buffer, respectively (Bossing et al., 2012; Schulman et al., 2013) (see also Fig. 7). In addition, although the non-specific background intensity that occurs with anti-β-Tubulin 97EF, as evident in *βTub97EF* null mutant hemocytes, was subtracted from signal intensities obtained in the other genotypes, the extent of non-specific background resulting with anti-α- and anti-β-tubulin could not be assessed and subtracted. Moreover, non-linearity of detection might vary between different antibodies. Despite these limitations, our signal quantification clearly revealed that expression of *UASt-βTub97EF(4B)* and *UASt-βTub56D* has distinct consequences in larval hemocytes. *UASt-βTub97EF(4B)* expression resulted in a pronounced increase of not only the signals obtained with anti-β-Tubulin 97EF and anti-β-tubulin, but also of those obtained with anti-α-tubulin (Fig. 6A, *R-97EF* and *S-97EF*). The anti-tubulin signals were particularly prominent in microtubule bundles in the peripheral region. In contrast, *UASt-βTub56D* expression resulted in a more limited increase in signal intensities (Fig. 6A, *R-56D* and *S-56D*). Therefore, β-Tubulin 97EF appears to stabilize microtubules. The post-transcriptional feedback preventing free tubulin heterodimer excess (Cleveland, 1988) likely contributes to the positive effect of *UASt-βTub97EF(4B)* expression on anti-α-tubulin signal intensity.

For additional comparison of the effects resulting from *UASt-βTub97EF(4B)* and *UASt-βTub56D* expression, we analyzed EB1-GFP comet movements. In *R-56D* and *S-56D* hemocytes, moving

Development (2017) 144, 4573-4587 doi:10.1242/dev.156109

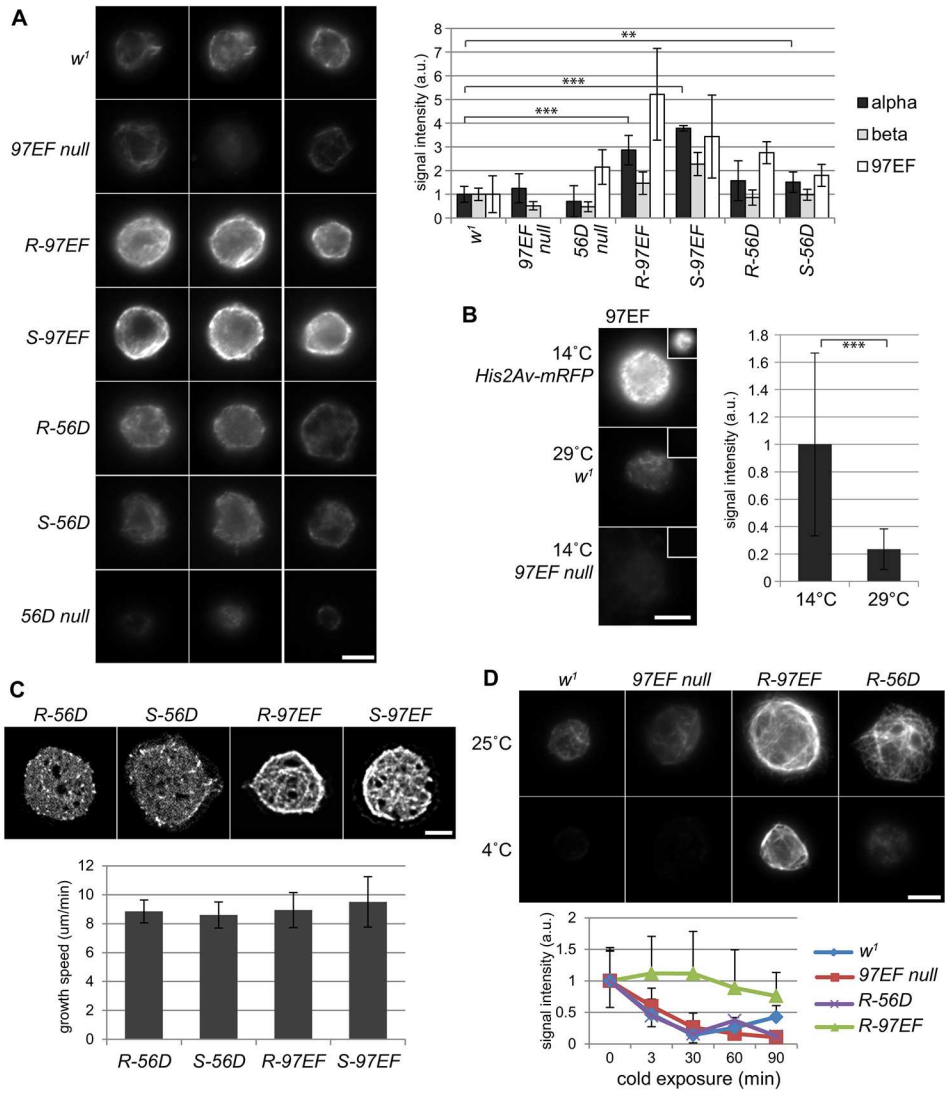

Fig. 6. β-Tubulin 97EF stabilizes microtubules in larval hemocytes. (A-D) Hemocytes were isolated from larvae with the indicated genotypes [97EF null=*βTub97EF*^{MiMIC}; 56D null=*βTub56D*^{NP0949}/*Df(2R)BSC782*; R-97EF and S-97EF=56D null and *Df(2R)BSC782*/balancer, respectively, with *αTub84BP>βTub97EF*; R-56D and S-56D=56D null and *Df(2R)BSC782*/balancer, respectively, with *αTub84BP>βTub56D*]. (A) Hemocytes were double labeled with anti-β-Tubulin 97E and anti-α-tubulin (left and middle columns) or only with anti-β-tubulin (E7) (right column). Data are mean±s.d. (n=11). Intensities obtained in *w*^{1} were set to 1. Statistically significant increases in the anti-α-tubulin signals are indicated (**P<0.01, ***P<0.001, t-test). (B) Hemocytes from larvae with the indicated genotypes after development at the indicated temperatures were released onto the same cover slip to enforce identical fixation and staining conditions. Nuclear His2Av-mRFP fluorescence (insets) was used for hemocyte classification. Bar diagrams indicate average background-corrected anti-β-Tubulin 97EF signal intensities (±s.d., n=20). Signals observed at 14°C in *w*^{1} were set to 1. ***P≤0.001 (t-test). (C) Representative still frames after time-lapse imaging of hemocytes expressing EB1-GFP. Bar diagram indicates average speed of EB1-GFP comet movements (±s.d., n=11). (D) Hemocytes of indicated genotypes were incubated at 4°C for the indicated time before fixation and staining using anti-α-tubulin. Graph represents average signal intensity (±s.d., n=10). Signals observed at time 0 h were set to 1 for each genotype. Scale bars: 5 µm.

EB1-GFP comets were readily observed (Fig. 6C, Movie 1), similar to those previously described in normal control hemocytes (Leśniewska et al., 2014). In contrast, EB1-GFP comets were far less evident in *R-97EF* and *S-97EF* hemocytes (Fig. 6C, Movie 1). In these cells, the mobile comets were partially masked by stably persisting EB1-GFP signals all along the microtubule network and most prominently at the cell cortex. Newly appearing EB1-GFP comets advanced mostly along the persisting bundles. Quantification of the dynamics of EB1-GFP comets did not reveal statistically significant differences in the effects of *UASt-βTub97EF(4B)* and *UASt-βTub56D* expression on the speed of EB1-GFP comet migration (Fig. 6C). These findings suggested that β-Tubulin 97EF increases the amount of microtubules, but not by stimulating the microtubule growth rate.

To further confirm that increased levels of β-Tubulin 97EF stabilize microtubules, we analyzed their cold sensitivity. As predicted, cold treatment was found to have a far greater destabilizing effect in hemocytes expressing *UASt-βTub56D* compared with those expressing *UASt-βTub97EF(4B)* (Fig. 6D). In *R-56D* hemocytes, anti-α-tubulin signals were already drastically lower after 3 min of incubation at 4°C. In contrast, signals were still high in *R-97EF* hemocytes even after 90 min at 4°C. Beyond cold sensitivity of microtubules, we also analyzed their colcemid sensitivity. Colcemid inhibits microtubule growth and depolymerizes microtubules at higher concentrations (Ravelli et al., 2004). As in the case of cold treatment, colcemid was found to have a higher destabilizing effect on hemocytes expressing *UASt-βTub56D* compared with those expressing *UASt-βTub97EF(4B)* (Fig. S10). Analogous analyses after expression of β-Tubulin 56D and 97EF with swapped C-terminal tails, indicated that the microtubule-stabilizing effect is mediated by the β-Tubulin 97EF core and not by its C-terminal tail (Fig. S10). All these results support the notion that β-Tubulin 97EF stabilizes microtubules.

The analysis of microtubules in hemocytes indicated that microtubules containing β-Tubulin 97EF are more stable than those built primarily from the major embryonic maternally provided β-Tubulin 56D. Accordingly, the hindgut microtubules of *βTub97EF* mutants (containing only maternally derived β-Tubulin 56D) are predicted to be less stable than those in wild-type control embryos (containing β-Tubulin 56D and β-Tubulin 97EF). To address this prediction, we performed microtubule depolymerization experiments with embryos with or without *βTub97EF* function. For these experiments, we used vinblastine because it depolymerized microtubules in embryos more effectively than colcemid (data not shown). After vinblastine or mock treatment, embryos were stained with anti-α-tubulin and signal intensities were quantified. The

Development (2017) 144, 4573-4587 doi:10.1242/dev.156109

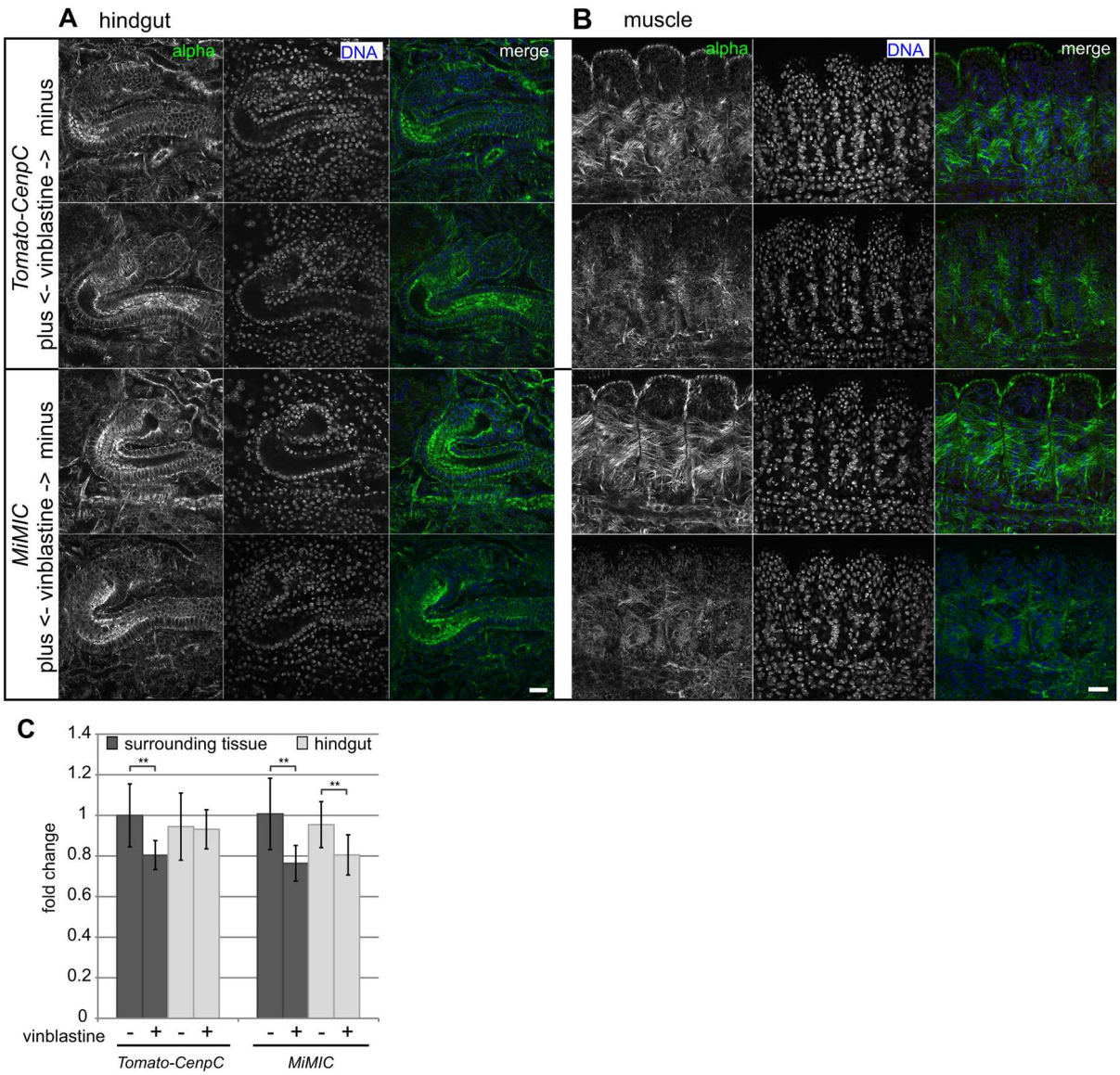

Fig. 7. Increased microtubule stability in the embryonic hindgut depends on *βTub97EF*. (A-C) Embryos (13-14 h AED) with or without *βTub97EF* gene function (*g-tdTomato-CenpC* and *MiMIC*, respectively) were exposed to vinblastine (+) or solvent only (–) before immunostaining using anti-α-tubulin. Sections illustrating the effect on anti-α-tubulin signal intensities in the hindgut and surrounding tissues (A) or in somatic muscles (B) are displayed. Scale bars: 15 µm. (C) Bar diagram representing average anti-α-tubulin signal intensities in the hindgut and in the surrounding tissues (±s.d., *n*=9). ***P*<0.01 (*t*-test). Signals in controls were set to 1.

quantification revealed that in the hindgut, vinblastine caused a significant reduction in the level of anti-α-tubulin signals but only in embryos lacking *βTub97EF* function (Fig. 7). In contrast, in the tissues surrounding the hindgut and in the body muscles, vinblastine reduced the level of anti-α-tubulin signals to a comparable extent in embryos with and without *βTub97EF* function (Fig. 7). These results indicate that microtubules in normal hindgut, where *βTub97EF* expression is high, are more stable than in tissues, where *βTub97EF* is, at most, marginally expressed. Moreover, this higher microtubule stability in the hindgut depends on *βTub97EF* expression, as it is lost in *βTub97EF* mutants.

DISCUSSION

The molecular mechanisms that allow acclimation to ambient temperature fluctuations are poorly understood. Here, we have identified *βTub97EF* as a temperature-responsive gene in *Drosophila melanogaster*. At low temperature, *βTub97EF* expression is increased. However, at the optimal temperature, as well as at lower temperatures, *βTub97EF* is not expressed ubiquitously but is restricted to a range of tissues, including gut epithelial cells and hemocytes. Mutations that eliminate *βTub97EF* function have a surprisingly mild effect, presumably reflecting functional redundancy with other co-expressed β-tubulin paralogs. But without β-Tubulin 97EF, microtubules are less stable. Conversely, microtubules are stabilized by increased *βTub97EF* expression. Moreover, within the well-tolerated temperature range, embryogenesis of *βTub97EF* mutants is more cold sensitive than heat sensitive. Therefore, upregulation of *βTub97EF* at low temperature might contribute to acclimation by stabilizing microtubules.

A detailed understanding of the *βTub97EF* contribution to the success of embryogenesis specifically at the lower end of the

Development (2017) 144, 4573-4587 doi:10.1242/dev.156109

compatible temperature range will require further work. Lack of β-Tubulin 97EF in the gut epithelia might impair yolk use during late embryogenesis at low temperature. It might also affect hemocyte functions (Wood and Martin, 2017). Hemocytes are important for innate immunity, which is unlikely to be relevant for successful embryogenesis. However, they also provide functions essential for embryogenesis. They scavenge apoptotic corpses that result from the abundant developmentally programmed cell death. Moreover, they are crucial for secretion and remodeling of much of the extracellular matrix in embryos.

Microtubules are ubiquitous and temperature change will affect them in all cells. Irrespective of temperature change, microtubule properties are carefully controlled in animal cells, not only by alterations in tubulin isoform composition, but also by myriads of interacting factors. Therefore, their characteristics are modified in different cell types and intracellular subsets to serve a wide range of functions. Acclimation of these diverse microtubule systems to temperature change is therefore likely demanding and impossible to achieve simply and exclusively by global upregulation of a single tubulin paralog. Presumably, tissue-specific upregulation of *βTub97EF* is one of many mechanisms for microtubule acclimation in *D. melanogaster*.

Beyond acclimation to low temperature, *βTub97EF* expression occurs also at optimal and elevated growth temperatures. *βTub97EF* is one of the five β-tubulin paralogs present in the genome of *D. melanogaster*, which contains also five α-tubulin paralogs. The human genome hosts almost twice as many α- and β-tubulin genes (9 and 8, respectively), and genetic analyses during the past 10 years have uncovered an increasing number of disease-associated mutations primarily in the context of neurological disease and cancer (Bahi-Buisson et al., 2014; Ludueña and Banerjee, 2008; Wang et al., 2017). Characterization of these tubulin genes and associated phenotypes, also in mouse models, has fully confirmed the conclusions from pioneering analyses of tubulin paralog functions in *D. melanogaster*. Tubulin paralogs have distinct but often partially overlapping patterns of expression and functions. The understanding of how amino acid sequence alterations affect tubulin function has progressed slowly. Production of pure recombinant tubulin isoforms in quantities sufficient for studies of microtubule polymerization and dynamics *in vitro* has been achieved only very recently (Pamula et al., 2016; Sirajuddin et al., 2014; Ti et al., 2016; Valenstein and Roll-Mecak, 2016; Vemu et al., 2016; Widlund et al., 2012). As the microtubule interactome in cells is highly complex (Hughes et al., 2008; Yu et al., 2016) phenotypic analyses *in vivo* will also remain important.

Here we have used a series of transgenes for *GAL4*-regulated expression of all the *D. melanogaster* β-tubulin paralogs. As the transgenes are identical except for the coding sequences, differential effects most likely reflect functional specialization at the protein level. Expression with *ey-GAL4* (and additional drivers including *en-GAL4* and *da-GAL4*, data not shown) indicated that excess *βTub97EF* is more toxic than an excess of the other β-tubulin paralogs. Moreover, *βTub97EF-4C* excess is more detrimental than *βTub97EF-4B* excess. These two *βTub97EF* isoforms, which result from mutually exclusive splicing of the fourth exon, differ at 13 positions within an internal segment of 40 amino acids, but their N- and C-terminal regions are identical. Sequence divergence between tubulin paralogs is generally most extensive within the tails, particularly C-terminally, where several distinct post-translational modifications also occur (Gadadhar et al., 2017; Janke, 2014; Yu et al., 2015). Therefore, the C-terminal tails (CTTs) are thought to make important paralog-specific contributions, as fully confirmed recently (Sirajuddin et al., 2014). Our comparison of the 97EF and 56D β-tubulins also revealed that CTTs contribute to paralog-specific function. Whereas 56D with an 97EF-CTT behaved like normal 56D, 97EF with an 56D-CTT had a toxicity intermediate between 97EF and 56D, suggesting that the β-Tubulin 97EF core and CTT cooperate, as demonstrated most elegantly with the 56D and 85D paralogs (Popodi et al., 2008). Beyond CTT contributions, differences within the tubulin core were found to have more profound effects. The core is responsible for the characteristic microtubule-stabilizing effect of β-Tubulin 97EF in larval hemocytes. Similarly, a study with chimeric tail-swapped human β-tubulins IIB and III concluded that differences between the cores were largely responsible for the different microtubule dynamics observed *in vitro* (Pamula et al., 2016).

It is not immediately evident why the MT-stabilizing β-Tubulin 97EF should be predominantly expressed in gut epithelia. Perhaps visceral musculature activity causes relatively large deformations in the gut tube, while such effects of other muscles might be more dampened by the exocuticle. β-Tubulin 97EF might also contribute towards minimization of cold-induced paracellular leakage from the gut, resulting in a loss of ion and water homeostasis, which is thought to make a significant contribution to lethality in response to cold (Denlinger and Lee, 2010; MacMillan et al., 2017).

Our results indicate that β-Tubulin 97EF expression does not affect the microtubule growth rate, but results in microtubules that are less prone to destabilization by cold, colcemid and vinblastine. In principle, the stabilizing effect of β-Tubulin 97EF might reflect a lower MT catastrophe and/or a higher rescue rate. It might involve interactions with GTP and its hydrolysis, with α-tubulin within the heterodimer, or lattice contacts within the polymer, or also with more peripheral components (MAPs, motors, modifying enzymes). As β-Tubulin 97EF appears to be enriched in peripheral microtubules, it might confer resistance against cortical factors that stimulate catastrophe. Peripheral enrichment was apparent after double labeling of larval hemocytes with anti-α-tubulin and anti-β-Tubulin 97EF. However, locally distinct epitope-masking effects, e.g. by CTT-associated proteins or modifications, are clearly not excluded. Judging from the pattern of microtubules induced by β-Tubulin 97EF overexpression in hemocytes, this tubulin might also facilitate microtubule bundling (Molodtsov et al., 2016). Interestingly, although ectopic *βTub60D* expression in the germline did not affect oogenesis, *βTub97EF* specifically blocked dumping of nurse cell cytoplasm into the oocyte during mid-oogenesis, i.e. long after the onset of ectopic expression. Although dumping is crucially dependent on actin and myosin, microtubule inhibitors do not block the dumping process, even though they clearly inhibit some aspects of transport from nurse cells to oocyte, (Gutzeit, 1986; Lu et al., 2016; Roth and Lynch, 2009; Wheatley et al., 1995; Huelsmann, 2013). An excess of cortical microtubule bundles caused by ectopic β-Tubulin 97EF might therefore inhibit dumping by interference with normal myosin-mediated contraction of the cortical actin network in nurse cells.

Evidently, further analyses will be required to evaluate our speculative proposals. It is clear, however, that β-Tubulin 97EF has interesting properties that are remarkably distinct from those of other *D. melanogaster* paralogs.

MATERIALS AND METHODS

Drosophila strains

Several stocks were obtained from the Bloomington Drosophila Stock Center (Indiana University) and the Kyoto Stock Center (Kyoto Institute of Technology): $βTub97EF^{MiMIC}$ (# 41519) (Venken et al., 2011),

Development (2017) 144, 4573-4587 doi:10.1242/dev.156109

βTub97EF^{MBO1877} (# 24452) and *βTub97EF*^{MBO3812} (# 24275) (Metaxakis et al., 2005), *βTub56D*^{EY12300} (# 20734) (Bellen et al., 2004), *Df(2R)BSC782* (# 27354) and *Df(3R)BSC460* (# 24964) (Cook et al., 2012), *βTub56D*^{NP0949} (# 103830) (Hayashi et al., 2002); *βTub97EF*^{EGFP} was obtained by converting *βTub97EF*^{MiMIC} as described previously (Venken et al., 2011) (see supplementary Materials and Methods for further details). Two strains with *UASt-Tub xy* transgenes were obtained from FlyORF (University of Zurich, Switzerland): *M{UAS-βTub85D.ORF}ZH-86Fb* (F001298) and *M{UAS-βTub97EF(4B).ORF}ZH-86Fb* (F001587) (Bischof et al., 2013). The additional *UASt-Tub* lines (*M{UAS-βTub56D.ORF}ZH-86Fb*, *M{UAS-βTub60D.ORF}ZH-86Fb*, *M{UAS-βTub65B.ORF}ZH-86Fb*, *M{UAS-βTub97EF(4C).ORF}ZH-86Fb*, *M{UAS-βTub56D-97EFtail.ORF}ZH-86Fb* and *M{UAS-βTub97EF(4B)-56Dtail.ORF}ZH-86Fb*, as well as the *UASp-Tub* lines *M{UASp-βTub97EF(4B).ORF}ZH-86Fb* and *M{UASp-βTub60D.ORF}ZH-86Fb* were generated using analogous approaches (Bischof et al., 2013) (see supplementary Materials and Methods for further details). *UASp-EB1-GFP* (Jankovics and Brunner, 2006) was kindly provided by D. Brunner (University of Zurich, Zurich, Switzerland). The GAL4 driver lines have been described previously: *ey-GAL4 (5/8)* (Hazelett et al., 1998), *matα4-GAL-VP16 (V2H)* (Hacker and Perrimon, 1998) and *αTub84BP-GAL4 (LL7)* (#5138) (Lee and Luo, 1999). *gi2xtdTomato-Cenp-C* II.3 (Althoff et al., 2012) was used as a marker and *w* as a control strain. *βTub97EF*^{MiMIC} was backcrossed for four generations to *w* before comparison of the temperature sensitivity of development.

For analysis of the extent of *βTub56D* mutant development supported by other β-tubulin paralogs, the following crosses were set up. Virgin *Df(2R)BSC782/ CyO, Dfd-YFP; UASt-βTubXY* [with XY=56D, 60D, 65B, 85D, 97EF(4C) or 97EF(4C)] were crossed with male w*; *βTub56D*^{NP0949}*/ CyO, Dfd-GMR-nvYFP*; *αTub84BP-GAL4/ TM6B, Hu, Dfd-YFP*. Eggs were collected from these crosses on either apple agar plates or in tubes with standard fly food. Collection plates were inspected at intervals under a fluorescence stereomicroscope, allowing identification of larvae without the *Dfd-YFP* balancer chromosomes.

The rate of larval hatching from eggs was determined as described previously (Radermacher et al., 2014). Eggs were collected for 60 min on apple agar plates at 25°C and aged at this temperature for 5 h. The collection plates with the eggs were then divided into sectors. The eggs present on one of the sectors were fixed immediately with methanol and stained with a DNA stain to determine the fraction of unfertilized eggs. The other sectors were shifted to different temperatures and the fraction of hatched and unhatched eggs was determined eventually with the help of a stereomicroscope. The hatch rate was calculated as the ratio of the number of hatched eggs to the total number of eggs deposited on the sector minus the number of unfertilized eggs. For the analysis of the rate of development to the adult stage, eggs were also collected for 60 min at 25°C followed by aging at this temperature for 5 h. Sectors of the collection plates with eggs that had been counted were then separated into bottles containing standard fly food and shifted to different temperatures. The number of eclosed flies was determined eventually. The eclosion rate was calculated as a ratio between the number of eclosed flies to the total number of eggs minus the number of unfertilized embryos.

Fertility tests were performed with flies of the following four genotypes: *βTub97EF*^{MBO1877}*/ Df(3R)BSC460*, *βTub97EF*^{MBO3812}*/ Df(3R)BSC460*, *βTub97EF*^{MiMIC}*/ Df(3R)BSC460* and *w*^{1} for control. To assay male fertility, three males (2 days old) of a given genotype were crossed to three *w*^{1} virgin females. Three replicate crosses were started for each genotype. Parents were discarded after 2 days and the number of eclosing adults was determined. Female fertility was analyzed analogously with crosses of three virgin females of a given genotype with three *w*^{1} males.

To evaluate high-salt sensitivity, eggs were collected for 1 day from parents that were either *w*^{1}*; βTub97EF*^{MiMIC}*/ TM3, Sb* or *w*^{1}*; +/ TM3, Sb* for control. Eggs were collected in bottles with either normal fly food or fly food containing 0.2 M or 0.4 M additional NaCl. Three replicate collections per condition and genotype were made. All eclosed progeny was counted and scored for presence or absence of *Sb*.

For analysis of hindgut L/R asymmetry in 12-16 h AED embryos, eggs collected from *βTub97EF*^{MiMIC} or *w*^{1} (for control) were fixed and stained using anti-Crumbs and Hoechst 33285. Hindgut looping was scored microscopically (Zeiss Cell Observer HS, 40×/0.75 objective). For analysis of hindgut L/R asymmetry in adults, young flies (0-1 day old) were kept for 6 h on food with 2.5% erioglaucine (Sigma, #861146), resulting in blue coloring of the fly gut. Hindgut looping was scored using a stereo microscope.

Transcript analyses

The S2R+ cells used for the analysis of temperature effects on the transcriptome were cultured as described previously (Radermacher et al., 2014). Aliquots were shifted 24 h after plating at 25°C to different temperatures (11, 14, 25 and 30°C). After 24 h, RNA was extracted, followed by probe synthesis and microarray hybridization (*Drosophila* gene expression 4×44K microarrays, G2519F-021791, Agilent Technologies). Three independent replicas were analyzed and after normalization of signal intensities across replicates, average hybridization signals were determined. In contrast to all other tubulin paralogs, signals for the testis-specific *βTub85D* paralog were too low to be included in the S2R+ transcriptome analysis (Fig. 1A). A comprehensive analysis of temperature effects on the transcriptome of S2R+ cells will be described in detail elsewhere. Further experimental details can be provided upon request.

For qRT-PCR analysis, S2R+ cells were treated in the same way as for the microarray experiments. For qRT-PCR analysis with *w*^{1} embryos, eggs were collected at 25°C for 3 h. After additional aging at 25°C for 3 h, they were shifted to 14, 25 and 30°C for 40, 10 or 8 h, respectively. As a result, embryos were all at stage 16 of embryogenesis, irrespective of the applied temperature regime. An aliquot of each sample was fixed for controlling the developmental stage after DNA staining by microscopy. Total RNA was extracted from cells and embryos. After cDNA synthesis, qRT-PCR was performed (see supplementary Materials and Methods for further details and Table S1 for primer sequences).

In situ hybridization

In situ hybridization was carried out according to standard procedures (Tautz and Pfeifle, 1989). Full-length antisense and sense probes were amplified from the LP10436 EST plasmid using the primer pairs FM89/FM77 and FM90/FM103, respectively (see Table S1 for primer sequences). Digoxigenin-labeled probes were generated by *in vitro* transcription with digoxigenin-labeled UTP (Roche) and detected using alkaline phosphatase-conjugated anti-digoxigenin Fab fragments (1:2000; Roche).

Antibodies

The rabbit antibodies against β-Tubulin 97EF were generated with a synthetic peptide corresponding to the last 17 amino acids (AEQEGYESEVLQNGNGE) coupled to KHL (Moravian Biotechnology). Antibodies were affinity purified. Rabbit antibodies against β-Tubulin 60D (Leiss et al., 1988) were kindly provided by R. Renkawitz-Pohl (University of Marburg, Germany). Further information on antibodies and dilutions applied during immunoblotting and immunolabeling is given in the supplementary Materials and Methods.

Immunoblotting

For a quantitative comparison of the sensitivity with which various anti-β-tubulin antibodies recognize the different *Drosophila* β-tubulin paralogs, we performed immunoblotting with total extracts prepared with bacteria expressing distinct GST protein variants with N- and C-terminal extensions corresponding to those of a particular β-tubulin paralog. Plasmid constructs based on the vector pET-21d (Novagen, Merck) were used for bacterial expression of the different GST fusion proteins (see supplementary Materials and Methods for further details).

Total extracts from cells, embryos, larvae and adults (see supplementary Materials and Methods for further details) were prepared for resolution by gel electrophoresis. Embryos and larvae aged at different temperatures were processed with solutions that had been pre-equilibrated to the temperatures used for aging. For probing samples with different anti-tubulin antibodies, separate gels and immunoblots were used for each antibody in order to avoid potential masking effects that might arise during serial probing of a single immunoblot. Immunoblot signals were developed using chemiluminescence (Amersham ECL) and captured using a CCD camera. For quantification of immunoblot signals, a dilution series of a

Development (2017) 144, 4573-4587 doi:10.1242/dev.156109

reference extract was resolved along with the test samples. Quantification of signals by densitometry was carried out using ImageJ as described previously (Radermacher et al., 2014).

Immunolabeling and microscopic analyses

For the majority of analyses with S2R+ cells, fixation was carried out with methanol containing 1 mM EGTA for 10 min at −20°C (Hoogenraad et al., 2000). Subsequent immunolabeling, as well as experiments with embryos, were carried as described previously (Radermacher et al., 2014).

To achieve maximal accuracy and minimize problems caused by potential fixation and staining artifacts in the experiments involving quantification of immunofluorescent signal intensities in embryos, these experiments were performed by combining four different types of stage 16 embryos before fixation and staining in a pool. Two of these embryo types were processed after development at 14°C. To identify these 'cold' embryos during the microscopic analyses, they were collected from strains expressing red fluorescent centromere protein Cenp-C (*gi2xtdTomato-Cenp-C* II.3). In contrast, the two other types, the 'warm' embryos, which were processed after development at a higher temperature (25°C or 30°C), did not have this marker transgene. Based on red fluorescent centromere signals 'cold' and 'warm' embryos were identified. Moreover, in order to quantify the level of non-specific signals resulting from anti-β-Tubulin 97EF labeling, both the 'cold' and the 'warm' embryos were a mixture of two different genotypes. Half of the embryos were $\beta Tub97EF^{MiMIC}$ mutants and the other half had two wild-type alleles of *βTub97EF*. Green fluorescent anti-β-Tubulin 97EF labeling revealed the *βTub97EF* genotype during the microscopic analyses. In addition, anti-α-tubulin labeling was visualized using a far-red fluorophore. In a second set of analogous experiments, *gi2xtdTomato-Cenp-C* II.3 was used for marking the 'warm' instead of the 'cold' embryos. Tissue-specific β-Tubulin 97EF upregulation in the hindgut at low temperature was observed in both sets of experiments (i.e. irrespective of whether *gi2xtdTomato-Cenp-C* II.3 was marking 'cold' or 'warm' embryos).

Pooling of embryos in combination with marking by *gi2xtdTomato-Cenp-C* II.3 was also carried out for the analysis of the effects of vinblastine treatment. Before onset of vinblastine or mock treatment, embryos with and without *βTub97EF* function were combined into a pool. To identify the different genotypes during the microscopic analysis eventually, the embryos with *βTub97EF* gene function had *gi2xtdTomato-Cenp-C* II.3. In contrast, the *βTub97EF* mutants did not have this marker transgene. *gi2xtdTomato-Cenp-C* II.3 and $\beta Tub97EF^{MiMIC}$ embryos were collected and aged to 11-13 h AED. Pooled embryos were dechorionated with 3% sodium hypochlorite, washed extensively with 0.7% NaCl and 0.07% Triton X-100, and transferred into an Eppendorf tube. 1.5 ml of a 1:1 mixture of heptane and Schneider's medium were added then 3 µl of a vinblastine (Sigma, V1377) stock solution (5 mM in methanol) or 3 µl methanol (control) aliquots were added. The Eppendorf tubes were slowly rotated end over end for 20 min at room temperature. Thereafter, embryos were fixed with methanol followed by immunolabeling.

Hemocytes were isolated as previously described (Sampson and Williams, 2012) using second instar larvae (*R-56D*, *S-56D*, *R-97EF*, *S-97EF*) or first instar larvae ($\beta Tub56D^{NP0949}$/ *Df(2R)BSC782*). The larvae were collected in a drop of 150 µl Schneider's medium on a glass slide that had been pre-coated with 0.5 mg/ml concanavaline A (Sigma, C7275) in phosphate buffer [9 mM NaH_2PO_4, 1 mM Na_2HPO_4, 1 mM $CaCl_2$ (pH 6.0)]. Larval cuticles were gently ruptured using forceps. This allowed migration of hemocytes out of the larvae and their subsequent initial attachment to the cover slip. After 15 min at room temperature, larvae were discarded. Before fixation or live imaging, hemocytes were allowed to spread during a 60 min incubation at 25°C.

In case of cold treatment, the 35 mm dishes with glass bottoms and spread hemocytes on top were incubated on the surface of an ice-water mixture for the desired time periods before fixation. In case of colcemid treatment, the compound was added to a final concentration of 10 µM in Schneider's medium. Hemocytes were fixed either with 4% paraformaldehyde in phosphate-buffered saline (PBS) at room temperature or (for Fig. 6D) with methanol containing 1 mM EGTA for 10 min at −20°C (Hoogenraad et al., 2000).

Images from fixed samples were acquired with an Olympus FluoView 1000 laser scanning confocal microscope with a 60×/1.35 objective and a 2× zoom for maximal magnification (Fig. 2C, Fig. 3D, Fig. 4C, Fig. 7A,B, Fig. S3E, Fig. S7A,C, Fig. S10), with a 40×/1.3 objective (Fig. S3B,C, Figs S5, S9) or with a Zeiss Cell Observer HS wide-field microscope with a 63×/1.4 objective (Fig. 2B,D, Fig. 6A,B,D, Fig. S8B), or with 16×/0.5 objective (Fig. 5C, Fig. S3A-C, Fig. S8B). *Z*-stacks were acquired. Single sections are presented in all images, except in Fig. 3A, where maximum intensity projections of relevant regions made with Imaris (Bitplane) are displayed. The intensities of anti-tubulin signals in hindgut in Fig. 4C-E were measured using ImageJ in maximum projections of five slices taken within the middle of the hindgut tube. The intensities of anti-α-tubulin staining in hindgut and other embryonic tissues (Fig. 7) were measured in single slices with ImageJ after manual selection of the regions of interest. Image *z*-stacks of eyes and embryos (Fig. 5B,D) and larvae (Fig. S8D) were acquired with a Zeiss AxioCam HRc camera and converted into extended focus images using Helicon Focus Software (Helicon Soft). This camera was also used for acquisition of embryos after *in situ* hybridization.

Time-lapse imaging of EB1-GFP comets in live hemocytes was carried out using a VisiScope spinning disc confocal microscope (Visitron) on an Olympus IX83 microscope stand with a 100×/1.4 objective. Three sections with 0.1 µm spacing were acquired at 1 s intervals. Signals in the case of *R-97EF* and *S-97EF* were deconvolved using Huygens Software (Scientific Volume Imaging). Quantification of microtubule dynamics after sum of intensity projections was carried out using u-track software (Jaqaman et al., 2008). To differentiate the moving EB1-GFP comet signals from the stationary EB1-GFP signals characteristically present in the *R-97EF* and *S-97EF* hemocytes along microtubule bundles, image sequences were processed arithmetically in ImageJ as follows. In a first variant image sequence, the first four frames were deleted. The last four frames were deleted in a second variant. By subtracting variant 2 from variant 1, we arrived at an image sequence from which background was subtracted (Image J, rolling ball radius two pixels) before analysis with u-track. Preparation and immunolabeling of organs from larvae (gut) and adults (gut, ovaries) were performed after fixation with 4% formaldehyde in PBS (see supplementary Materials and Methods for further details).

Hindgut ultrastructure in w^1 and $\beta Tub97EF^{MiMIC}$ after development at 25°C to 15-16 h AED was characterized by transmission electron microscopy and FIBSEM (see supplementary Materials and Methods for further details).

Acknowledgements

We thank Renate Renkawitz-Pohl for anti-β-Tubulin 60D and Nikola Linsi for his contributions to antibody characterization. We are also grateful to Rita Lecca and the Functional Genomics Center Zurich for supporting microarray hybridizations, to Martin Moser for qRT-PCR support, as well as to Andres Käch and the Center for Microscopy and Image Analysis (University of Zurich).

Competing interests

The authors declare no competing or financial interests.

Author contributions

Conceptualization: C.F.L.; Methodology: F.M., F.B., C.F.L.; Software: F.B.; Validation: F.M., F.B., C.F.L.; Formal analysis: F.M., F.B.; Investigation: F.M., F.B., M.K.; Resources: F.M., J.B.; Data curation: F.B.; Writing - original draft: C.F.L.; Writing - review & editing: F.M., C.F.L.; Visualization: F.M., M.K., C.F.L.; Supervision: C.F.L.; Project administration: C.F.L.; Funding acquisition: C.F.L.

Funding

This work was supported by the Schweizerischer Nationalfonds zur Förderung der Wissenschaftlichen Forschung (31003A_152667 to C.F.L.).

Supplementary information

Supplementary information available online at
http://dev.biologists.org/lookup/doi/10.1242/dev.156109.supplemental

References

Althoff, F., Karess, R. E. and Lehner, C. F. (2012). Spindle checkpoint-independent inhibition of mitotic chromosome segregation by Drosophila Mps1. *Mol. Biol. Cell* **23**, 2275-2291.

Bahi-Buisson, N., Poirier, K., Fourniol, F., Saillour, Y., Valence, S., Lebrun, N., Hully, M., Fallet Bianco, C., Boddaert, N., Elie, C. et al. (2014). The wide

spectrum of tubulinopathies: what are the key features for the diagnosis? *Brain* **137**, 1676-1700.
Bellen, H. J., Levis, R. W., Liao, G., He, Y., Carlson, J. W., Tsang, G., Evans-Holm, M., Hiesinger, P. R., Schulze, K. L., Rubin, G. M. et al. (2004). The BDGP gene disruption project: single transposon insertions associated with 40% of Drosophila genes. *Genetics* **167**, 761-781.
Bischof, J., Bjorklund, M., Furger, E., Schertel, C., Taipale, J. and Basler, K. (2013). A versatile platform for creating a comprehensive UAS-ORFeome library in Drosophila. *Development* **140**, 2434-2442.
Blose, S. H., Meltzer, D. I. and Feramisco, J. R. (1984). 10-nm filaments are induced to collapse in living cells microinjected with monoclonal and polyclonal antibodies against tubulin. *J. Cell Biol.* **98**, 847-858.
Bossing, T., Barros, C. S., Fischer, B., Russell, S. and Shepherd, D. (2012). Disruption of microtubule integrity initiates mitosis during CNS repair. *Dev. Cell* **23**, 433-440.
Breitling, F. and Little, M. (1986). Carboxy-terminal regions on the surface of tubulin and microtubules epitope locations of YOL1/34, DM1A and DM1B. *J. Mol. Biol.* **189**, 367-370.
Buttgereit, D., Leiss, D., Michiels, F. and Renkawitz-Pohl, R. (1991). During Drosophila embryogenesis the beta 1 tubulin gene is specifically expressed in the nervous system and the apodemes. *Mech. Dev.* **33**, 107-118.
Buttgereit, D., Paululat, A. and Renkawitz-Pohl, R. (1996). Muscle development and attachment to the epidermis is accompanied by expression of beta 3 and beta 1 tubulin isotypes, respectively. *Int. J. Dev. Biol.* **40**, 189-196.
Cherbas, L., Willingham, A., Zhang, D., Yang, L., Zou, Y., Eads, B. D., Carlson, J. W., Landolin, J. M., Kapranov, P., Dumais, J. et al. (2011). The transcriptional diversity of 25 Drosophila cell lines. *Genome Res.* **21**, 301-314.
Chiappori, F., Pucciarelli, S., Merelli, I., Ballarini, P., Miceli, C. and Milanesi, L. (2012). Structural thermal adaptation of beta-tubulins from the Antarctic psychrophilic protozoan Euplotes focardii. *Proteins* **80**, 1154-1166.
Chu, D. T. W. and Klymkowsky, M. W. (1989). The appearance of acetylated α-tubulin during early development and cellular differentiation in Xenopus. *Dev. Biol.* **136**, 104-117.
Cleveland, D. W. (1988). Autoregulated instability of tubulin mRNAS: a novel eukaryotic regulatory mechanism. *Trends Biochem. Sci.* **13**, 339-343.
Cook, R. K., Christensen, S. J., Deal, J. A., Coburn, R. A., Deal, M. E., Gresens, J. M., Kaufman, T. C. and Cook, K. R. (2012). The generation of chromosomal deletions to provide extensive coverage and subdivision of the Drosophila melanogaster genome. *Genome Biol.* **13**, R21.
Correia, J. J. and Williams, R. C. (1983). Mechanisms of assembly and disassembly of microtubules. *Annu. Rev. Biophys. Bioeng.* **12**, 211-235.
Coutelis, J.-B., González-Morales, N., Géminard, C. and Noselli, S. (2014). Diversity and convergence in the mechanisms establishing L/R asymmetry in metazoa. *EMBO Rep.* **15**, 926-937.
Delphin, C., Bouvier, D., Seggio, M., Couriol, E., Saoudi, Y., Denarier, E., Bosc, C., Valiron, O., Bisbal, M., Arnal, I. et al. (2012). MAP6-F is a temperature sensor that directly binds to and protects microtubules from cold-induced depolymerization. *J. Biol. Chem.* **287**, 35127-35138.
Denlinger, D. L. and Lee, R. E. (2010). *Low Temperature Biology of Insects*. Cambridge: Cambridge University Press.
Detrich, H. W., III, Parker, S. K., Williams, R. C., Jr., Nogales, E. and Downing, K. H. (2000). Cold adaptation of microtubule assembly and dynamics. Structural interpretation of primary sequence changes present in the alpha- and beta-tubulins of Antarctic fishes. *J. Biol. Chem.* **275**, 37038-37047.
Findeisen, P., Mühlhausen, S., Dempewolf, S., Hertzog, J., Zietlow, A., Carlomagno, T. and Kollmar, M. (2014). Six Subgroups and extensive recent duplications characterize the evolution of the eukaryotic tubulin protein family. *Genome Biol. Evol.* **6**, 2274-2288.
Fuller, M. T., Caulton, J. H., Hutchens, J. A., Kaufman, T. C. and Raff, E. C. (1988). Mutations that encode partially functional beta 2 tubulin subunits have different effects on structurally different microtubule arrays. *J. Cell Biol.* **107**, 141-152.
Fygenson, D. K., Braun, E. and Libchaber, A. (1994). Phase diagram of microtubules. *Phys. Rev. E* **50**, 1579-1588.
Gadadhar, S., Bodakuntla, S., Natarajan, K. and Janke, C. (2017). The tubulin code at a glance. *J. Cell Sci.* **130**, 1347-1353.
Gasch, A. P., Spellman, P. T., Kao, C. M., Carmel-Harel, O., Eisen, M. B., Storz, G., Botstein, D. and Brown, P. O. (2000). Genomic expression programs in the response of yeast cells to environmental changes. *Mol. Biol. Cell* **11**, 4241-4257.
Graveley, B. R., Brooks, A. N., Carlson, J. W., Duff, M. O., Landolin, J. M., Yang, L., Artieri, C. G., van Baren, M. J., Boley, N., Booth, B. W. et al. (2011). The developmental transcriptome of Drosophila melanogaster. *Nature* **471**, 473-479.
Gutzeit, H. (1986). The role of microtubules in the differentiation of ovarian follicles during vitellogenesis in Drosophila. *Roux. Arch. Dev. Biol.* **195**, 173-181.
Hacker, U. and Perrimon, N. (1998). DRhoGEF2 encodes a member of the Dbl family of oncogenes and controls cell shape changes during gastrulation in Drosophila. *Genes Dev.* **12**, 274-284.
Hayashi, S., Ito, K., Sado, Y., Taniguchi, M., Akimoto, A., Takeuchi, H., Aigaki, T., Matsuzaki, F., Nakagoshi, H., Tanimura, T. et al. (2002). GETDB, a database compiling expression patterns and molecular locations of a collection of gal4 enhancer traps. *Genesis* **34**, 58-61.
Hayward, S. A. L., Murray, P. A., Gracey, A. Y. and Cossins, A. R. (2007). Beyond the lipid hypothesis: mechanisms underlying phenotypic plasticity in inducible cold tolerance. *Adv. Exp. Med. Biol.* **594**, 132-142.
Hazelett, D. J., Bourouis, M., Walldorf, U. and Treisman, J. E. (1998). decapentaplegic and wingless are regulated by eyes absent and eyegone and interact to direct the pattern of retinal differentiation in the eye disc. *Development* **125**, 3741-3751.
Hoogenraad, C. C., Akhmanova, A., Grosveld, F., De Zeeuw, C. I. and Galjart, N. (2000). Functional analysis of CLIP-115 and its binding to microtubules. *J. Cell Sci.* **113**, 2285-2297.
Hoyle, H. D. and Raff, E. C. (1990). Two Drosophila beta tubulin isoforms are not functionally equivalent. *J. Cell Biol.* **111**, 1009-1026.
Hughes, J. R., Meireles, A. M., Fisher, K. H., Garcia, A., Antrobus, P. R., Wainman, A., Zitzmann, N., Deane, C., Ohkura, H. and Wakefield, J. G. (2008). A microtubule interactome: complexes with roles in cell cycle and mitosis. *PLoS Biol.* **6**, e98.
Iwaki, D. D. and Lengyel, J. A. (2002). A Delta–Notch signaling border regulated by Engrailed/Invected repression specifies boundary cells in the Drosophila hindgut. *Mech. Dev.* **114**, 71-84.
Janke, C. (2014). The tubulin code: molecular components, readout mechanisms, and functions. *J. Cell Biol.* **206**, 461-472.
Jankovics, F. and Brunner, D. (2006). Transiently reorganized microtubules are essential for zippering during dorsal closure in Drosophila melanogaster. *Dev. Cell* **11**, 375-385.
Jaqaman, K., Loerke, D., Mettlen, M., Kuwata, H., Grinstein, S., Schmid, S. L. and Danuser, G. (2008). Robust single-particle tracking in live-cell time-lapse sequences. *Nat. Meth.* **5**, 695-702.
Kemphues, K. J., Kaufman, T. C., Raff, R. A. and Raff, E. C. (1982). The testis-specific β-tubulin subunit in Drosophila melanogaster has multiple functions in spermatogenesis. *Cell* **31**, 655-670.
Kimble, M., Incardona, J. P. and Raff, E. C. (1989). A variant beta-tubulin isoform of Drosophila melanogaster (beta 3) is expressed primarily in tissues of mesodermal origin in embryos and pupae, and is utilized in populations of transient microtubules. *Dev. Biol.* **131**, 415-429.
Kimble, M., Dettman, R. W. and Raff, E. C. (1990). The beta-3-tubulin gene of Drosophila-melanogaster is essential for viability and fertility. *Genetics* **126**, 991-1005.
Kumichel, A. and Knust, E. (2014). Apical localisation of crumbs in the boundary cells of the drosophila hindgut is independent of its canonical interaction partner stardust. *PLoS ONE* **9**, e94038.
Lee, T. and Luo, L. (1999). Mosaic analysis with a repressible cell marker for studies of gene function in neuronal morphogenesis. *Neuron* **22**, 451-461.
Leiss, D., Hinz, U., Gasch, A., Mertz, R. and Renkawitz-Pohl, R. (1988). Beta 3 tubulin expression characterizes the differentiating mesodermal germ layer during Drosophila embryogenesis. *Development* **104**, 525-531.
Leśniewska, K., Warbrick, E. and Ohkura, H. (2014). Peptide aptamers define distinct EB1- and EB3-binding motifs and interfere with microtubule dynamics. *Mol. Biol. Cell* **25**, 1025-1036.
Lu, W., Winding, M., Lakonishok, M., Wildonger, J. and Gelfand, V. I. (2016). Microtubule–microtubule sliding by kinesin-1 is essential for normal cytoplasmic streaming in Drosophila oocytes. *Proc. Natl Acad. Sci. USA* **113**, E4995-E5004.
Ludueña, R. and Banerjee, A. (2008). The isotypes of tubulin. In *The Role of Microtubules in Cell Biology, Neurobiology, and Oncology* (ed. T. Fojo), pp. 123-175. New York, NY: Humana Press.
MacMillan, H. A., Yerushalmi, G. Y., Jonusaite, S., Kelly, S. P. and Donini, A. (2017). Thermal acclimation mitigates cold-induced paracellular leak from the Drosophila gut. *Sci. Rep.* **7**, 8807.
Metaxakis, A., Oehler, S., Klinakis, A. and Savakis, C. (2005). Minos as a genetic and genomic tool in Drosophila melanogaster. *Genetics* **171**, 571-581.
Mimori-Kiyosue, Y., Shiina, N. and Tsukita, S. (2000). The dynamic behavior of the APC-binding protein EB1 on the distal ends of microtubules. *Curr. Biol.* **10**, 865-868.
Mitchison, T. and Kirschner, M. (1984). Dynamic instability of microtubule growth. *Nature* **312**, 237-242.
Modig, C., Wallin, M. and Olsson, P.-E. (2000). Expression of cold-adapted beta-tubulins confer cold-tolerance to human cellular microtubules. *Biochem. Biophys. Res. Commun.* **269**, 787-791.
Molodtsov, M. I., Mieck, C., Dobbelaere, J., Dammermann, A., Westermann, S. and Vaziri, A. (2016). A force-induced directional switch of a molecular motor enables parallel microtubule bundle Formation. *Cell* **167**, 539-552.e514.
Nogales, E. and Zhang, R. (2016). Visualizing microtubule structural transitions and interactions with associated proteins. *Curr. Opin. Struct. Biol.* **37**, 90-96.
Pamula, M. C., Ti, S.-C. and Kapoor, T. M. (2016). The structured core of human β tubulin confers isotype-specific polymerization properties. *J. Cell Biol.* **213**, 425-433.
Popodi, E. M., Hoyle, H. D., Turner, F. R. and Raff, E. C. (2008). Cooperativity between the β-tubulin carboxy tail and the body of the molecule is required for microtubule function. *Cell Motil. Cytoskelet.* **65**, 955-963.

Development (2017) 144, 4573-4587 doi:10.1242/dev.156109

Radermacher, P. T., Myachina, F., Bosshardt, F., Pandey, R., Mariappa, D., Muller, H.-A. J. and Lehner, C. F. (2014). O-GlcNAc reports ambient temperature and confers heat resistance on ectotherm development. *Proc. Natl. Acad. Sci. USA* **111**, 5592-5597.

Ravelli, R. B. G., Gigant, B., Curmi, P. A., Jourdain, I., Lachkar, S., Sobel, A. and Knossow, M. (2004). Insight into tubulin regulation from a complex with colchicine and a stathmin-like domain. *Nature* **428**, 198-202.

Roth, S. and Lynch, J. A. (2009). Symmetry breaking during drosophila oogenesis. *Cold Spring Harbor Perspect. Biol.* **1**, a001891.

Rudolf, A., Buttgereit, D., Rexer, K.-H. and Renkawitz-Pohl, R. (2012). The syncytial visceral and somatic musculature develops independently of β3-Tubulin during Drosophila embryogenesis, while maternally supplied β1-Tubulin is stable until the early steps of myoblast fusion. *Eur. J. Cell Biol.* **91**, 192-203.

Sampson, C. J. and Williams, M. J. (2012). Protocol for ex vivo incubation of Drosophila primary post-embryonic haemocytes for real-time analyses. In *Rho GTPases: Methods and Protocols* (ed. F. Rivero), pp. 359-367. New York, NY: Springer.

Schulman, V. K., Folker, E. S. and Baylies, M. K. (2013). A method for reversible drug delivery to internal tissues of Drosophila embryos. *Fly* **7**, 193-203.

Sirajuddin, M., Rice, L. M. and Vale, R. D. (2014). Regulation of microtubule motors by tubulin isotypes and post-translational modifications. *Nat. Cell Biol.* **16**, 335-344.

Soplop, N. H., Cheng, Y.-S. and Kramer, S. G. (2012). Roundabout is required in the visceral mesoderm for proper microvillus length in the hindgut epithelium. *Dev. Dyn.* **241**, 759-769.

Tartaglia, L. J. and Shain, D. H. (2008). Cold-adapted tubulins in the glacier ice worm, Mesenchytraeus solifugus. *Gene* **423**, 135-141.

Tautz, D. and Pfeifle, C. (1989). A non-radioactive in situ hybridization method for the localization of specific RNAs in Drosophila embryos reveals translational control of the segmentation gene hunchback. *Chromosoma* **98**, 81-85.

Taymaz-Nikerel, H., Cankorur-Cetinkaya, A. and Kirdar, B. (2016). Genome-wide transcriptional response of saccharomyces cerevisiae to stress-induced perturbations. *Front. Bioeng. Biotechnol.* **4**, 17.

Ti, S.-C., Pamula, M. C., Howes, S. C., Duellberg, C., Cade, N. I., Kleiner, R. E., Forth, S., Surrey, T., Nogales, E. and Kapoor, T. M. (2016). Mutations in human tubulin proximal to the kinesin-binding site alter dynamic instability at microtubule plus- and minus-ends. *Dev. Cell* **37**, 72-84.

Valenstein, M. L. and Roll-Mecak, A. (2016). Graded control of microtubule severing by tubulin glutamylation. *Cell* **164**, 911-921.

Vemu, A., Atherton, J., Spector, J. O., Szyk, A., Moores, C. A. and Roll-Mecak, A. (2016). Structure and dynamics of single-isoform recombinant neuronal human tubulin. *J. Biol. Chem.* **291**, 12907-12915.

Venken, K. J. T., Schulze, K. L., Haelterman, N. A., Pan, H., He, Y., Evans-Holm, M., Carlson, J. W., Levis, R. W., Spradling, A. C., Hoskins, R. A. et al. (2011). MiMIC: a highly versatile transposon insertion resource for engineering Drosophila melanogaster genes. *Nat. Methods* **8**, 737-743.

Wang, W., Zhang, H., Wang, X., Patterson, J., Winter, P., Graham, K., Ghosh, S., Lee, J. C., Katsetos, C. D., Mackey, J. R. et al. (2017). Novel mutations involving βI-, βIIA-, or βIVB-tubulin isotypes with functional resemblance to βIII-tubulin in breast cancer. *Protoplasma* **254**, 1163-1173.

Wheatley, S., Kulkarni, S. and Karess, R. (1995). Drosophila nonmuscle myosin-ii is required for rapid cytoplasmic transport during oogenesis and for axial nuclear migration in early embryos. *Development* **121**, 1937-1946.

Widlund, P. O., Podolski, M., Reber, S., Alper, J., Storch, M., Hyman, A. A., Howard, J. and Drechsel, D. N. (2012). One-step purification of assembly-competent tubulin from diverse eukaryotic sources. *Mol. Biol. Cell* **23**, 4393-4401.

Wood, W. and Martin, P. (2017). macrophage functions in tissue patterning and disease: new insights from the fly. *Dev. Cell* **40**, 221-233.

Yu, I., Garnham, C. P. and Roll-Mecak, A. (2015). Writing and reading the tubulin code. *J. Biol. Chem.* **290**, 17163-17172.

Yu, N., Signorile, L., Basu, S., Ottema, S., Lebbink, J. H. G., Leslie, K., Smal, I., Dekkers, D., Demmers, J. and Galjart, N. (2016). Isolation of functional tubulin dimers and of tubulin-associated proteins from mammalian cells. *Curr. Biol.* **26**, 1728-1736.

Zhang, R., Alushin, G. M., Brown, A. and Nogales, E. (2015). Mechanistic origin of microtubule dynamic instability and its modulation by EB proteins. *Cell* **162**, 849-859.